

AD-A130 535

POINT-MASS MODELING OF THE GRAVITY FIELD WITH EMPHASIS  
ON THE OCEANIC GEOID(U) NOVA UNIV OCEANOGRAPHIC CENTER  
DANIA FL G BLAHA FEB 83 AFGL-TR-83-0007

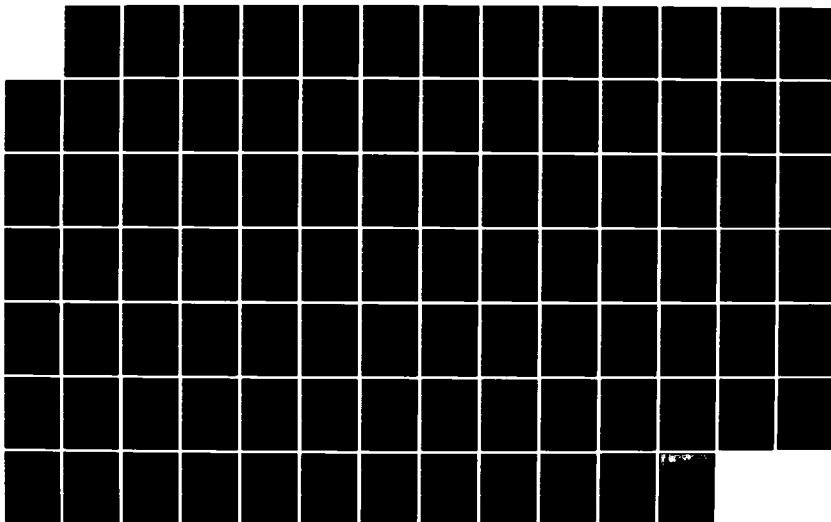
1/1

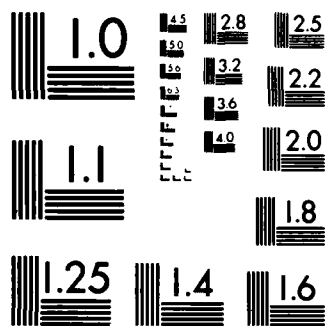
UNCLASSIFIED

F19628-82-K-0007

.F/G 8/5

NL





MICROCOPY RESOLUTION TEST CHART  
NATIONAL BUREAU OF STANDARDS-1963-A

AFGL-TR-83-0007

POINT-MASS MODELING OF THE GRAVITY FIELD  
WITH EMPHASIS ON THE OCEANIC GEOID

Georges Blaha

Nova University Oceanographic Center  
8000 North Ocean Drive  
Dania, Florida 33004

Scientific Report No. 1

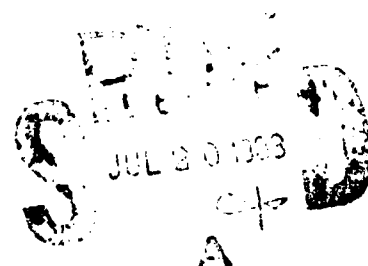
February 1983

Approved for public release; distribution unlimited

AD A130535

DTIC FILE COPY

AIR FORCE GEOPHYSICS LABORATORY  
AIR FORCE SYSTEMS COMMAND  
UNITED STATES AIR FORCE  
HANSCOM AFB, MASSACHUSETTS 01731




88 20 033

CONTRACTOR REPORTS

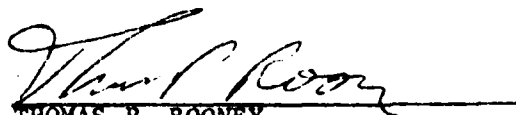
This report has been reviewed by the ESD Public Affairs Office (PA) and is releasable to the National Technical Information Service (NTIS).

This technical report has been reviewed and is approved for publication.

  
GEORGE HADGIGEORGE  
Contract Manager

  
THOMAS P. ROONEY  
Branch Chief

FOR THE COMMANDER

  
THOMAS P. ROONEY  
Acting Division Director

Qualified requestors may obtain additional copies from the Defense Technical Information Center. All others should apply to the National Technical Information Service.

If your address has changed, or if you wish to be removed from the mailing list, or if the addressee is no longer employed by your organization, please notify AFGL/DAA, Hanscom AFB, MA 01731. This will assist us in maintaining a current mailing list.

Do not return copies of this report unless contractual obligations or notices on a specific document requires that it be returned.

Unclassified

SECURITY CLASSIFICATION OF THIS PAGE (When Data Entered)

REPORT DOCUMENTATION PAGE		READ INSTRUCTIONS BEFORE COMPLETING FORM												
1. REPORT NUMBER AFGL-TR-83-0007	2. GOVT ACCESSION NO. AD A130 425	3. RECIPIENT'S CATALOG NUMBER												
4. TITLE (and Subtitle) POINT-MASS MODELING OF THE GRAVITY FIELD WITH EMPHASIS ON THE OCEANIC GEOID		5. TYPE OF REPORT & PERIOD COVERED Scientific Report No. 1 Period covered 1/1/82-12/31/82												
7. AUTHOR(s) Georges Blaha		6. PERFORMING ORG. REPORT NUMBER												
9. PERFORMING ORGANIZATION NAME AND ADDRESS Nova University Oceanographic Center 8000 North Ocean Drive Dania, Florida 33004		8. CONTRACT OR GRANT NUMBER(s) F19628-82-K-0007												
11. CONTROLLING OFFICE NAME AND ADDRESS Air Force Geophysics Laboratory Hanscom AFB, Massachusetts 01731 Contract Monitor: George Haddigeorge/LWG		10. PROGRAM ELEMENT, PROJECT, TASK AREA & WORK UNIT NUMBERS 61102F 2309G1BB												
14. MONITORING AGENCY NAME & ADDRESS (if different from Controlling Office)		12. REPORT DATE February 1983												
		13. NUMBER OF PAGES 91												
		15. SECURITY CLASS. (of this report) Unclassified												
		15a. DECLASSIFICATION/DOWNGRADING SCHEDULE												
16. DISTRIBUTION STATEMENT (of this Report) Approved for public release; distribution unlimited.														
17. DISTRIBUTION STATEMENT (of the abstract entered in Block 20, if different from Report)														
18. SUPPLEMENTARY NOTES														
19. KEY WORDS (Continue on reverse side if necessary and identify by block number) <table border="0"> <tr> <td>Satellite altimetry</td> <td>Deflection rates</td> <td>Diurnal constituents</td> </tr> <tr> <td>Geoid undulations</td> <td>Single point masses</td> <td>Semidiurnal constituents</td> </tr> <tr> <td>Gravity anomalies</td> <td>Twin point masses</td> <td>Least-squares adjustment</td> </tr> <tr> <td>Deflections of the vertical</td> <td>Tidal effects</td> <td>Normal equations</td> </tr> </table>			Satellite altimetry	Deflection rates	Diurnal constituents	Geoid undulations	Single point masses	Semidiurnal constituents	Gravity anomalies	Twin point masses	Least-squares adjustment	Deflections of the vertical	Tidal effects	Normal equations
Satellite altimetry	Deflection rates	Diurnal constituents												
Geoid undulations	Single point masses	Semidiurnal constituents												
Gravity anomalies	Twin point masses	Least-squares adjustment												
Deflections of the vertical	Tidal effects	Normal equations												
20. ABSTRACT (Continue on reverse side if necessary and identify by block number) <p>The satellite altimeter adjustments recently performed at AFGL are based on the short-arc algorithm, where the arcs' lengths have been limited to seven minutes or less and the data consist of SEASAT altimeter observations. The smoothed surface approximating the geoid is described by a truncated set of spherical-harmonic (S.H.) potential coefficients and each satellite arc is described by six state vector parameters considered independent from arc to</p>														

DD FORM 1 JAN 73 1473

EDITION OF 1 NOV 65 IS OBSOLETE

Unclassified

SECURITY CLASSIFICATION OF THIS PAGE (When Data Entered)

arc. Certain tidal effects are also included in the adjustment. However, each diurnal and semidiurnal constituent considered is attributed only two adjustable parameters: a global amplitude factor and a global phase angle correction. These parameters are shown to be essentially uncontaminated by the geoidal errors or by the systematic orbital errors. Such advantages would not exist if the adjustment were made in terms of S.H. tidal coefficients whose a priori values are used in the present model to describe the approximate behavior of the pertinent diurnal or semidiurnal constituents. The above two parameters represent very special linear combinations of these coefficients.

The inclusion of the tidal adjustment in the overall adjustment of satellite altimetry improves the geoidal residuals as well as the "observed" geoid undulations obtained by superimposing the former on the adjusted smooth geoid. Such "observed" values can serve to produce a high-degree and order set of S.H. potential coefficients via integral formulas (not via an adjustment), which can then serve in predicting the desired geophysical quantities. The geoidal residuals can be used as observations in a subsequent, or second-phase, adjustment of a short-wavelength oceanic geoid in terms of point-mass (P.M.) magnitudes as parameters. An important part of the development is concerned with a reformulation of the second-phase adjustment in terms of P.M. parameters, leading to a banded system of normal equations. Such a system can be arrived at and resolved by addressing three separate tasks in what can be called a "modified Choleski algorithm": 1) the elimination of the point masses from an observation equation if they are sufficiently far from the pertinent observation point, 2) the special arrangement of the P.M. parameters in the adjustment scheme, and 3) the resolution of the resulting system through an adaptation of the well-known Choleski algorithm. Whereas previously only small areas could be resolved in a P.M. approach, the oceanic geoid over entire ocean basins can now be adjusted in a few overlapping strips of point masses by virtue of a several-fold reduction in the run-time and core-space requirements achieved with the modified Choleski algorithm.

In a separate task, a model for the deflection rates along a given route is developed in tensor notations, and is subsequently specialized for the S.H. and P.M. parameters. It is pointed out that the rate of change in  $\xi$  when proceeding eastward minus the rate of change in  $\eta$  when proceeding northward yields a simple relationship which can serve as a useful mathematical verification at either level. The deflection rates as well as the observational modes developed and described in the previous AFGL reports are further presented in a different P.M. model. In particular, they are transformed from the context of single point masses to the context of twin point masses (the former implies a single P.M. layer while the latter implies a double P.M. layer). An analysis of all the observational modes considered confirms the plausible property that if a single point mass is made into a twin point mass, the effect exercised on a modeled value decreases much more rapidly with distance.

# TABLE OF CONTENTS

<u>CHAPTER</u>	<u>SECTION</u>	<u>DESCRIPTION</u>	<u>PAGE NO.</u>
		ABSTRACT	i
1		INTRODUCTION	1
2		ROLE OF THE TIDAL ADJUSTMENT IN COMPUTING THE "OBSERVED" GEOID AS THE BASIS FOR A DETAILED GRAVITY FIELD REPRESENTATION	5
	2.1	<u>General Discussion</u>	5
	2.2	<u>Effect of Tidal Modeling on the SEASAT Altimeter Adjustment</u>	13
	2.3	<u>Summary and Assessment of the "Observed" Geoid</u>	19
3		LARGE AREA ADJUSTMENT USING THE POINT MASS PARAMETERS	22
	3.1	<u>Notes on the Strategy in Choosing the Depth-Side Ratio of Point Masses</u>	22
	3.2	<u>Point-Mass Algorithm for a Banded System of Normal Equations</u>	28
4		MODEL FOR DEFLECTION RATES IN TERMS OF SPHERICAL HARMONICS AND POINT MASSES	44
	4.1	<u>Mathematical Background</u>	45
	4.2	<u>Spherical-Harmonic Approach</u>	50
	4.3	<u>Approach Using a Single Layer of Point Masses</u>	53
5		OBSERVATION MODES IN TERMS OF A DOUBLE LAYER OF POINT MASSES	61
	5.1	<u>Adaptation of Five Observational Modes to Twin Point Masses</u>	63
	5.2	<u>Development of Deflection Rates in Terms of Twin Point Masses</u>	73

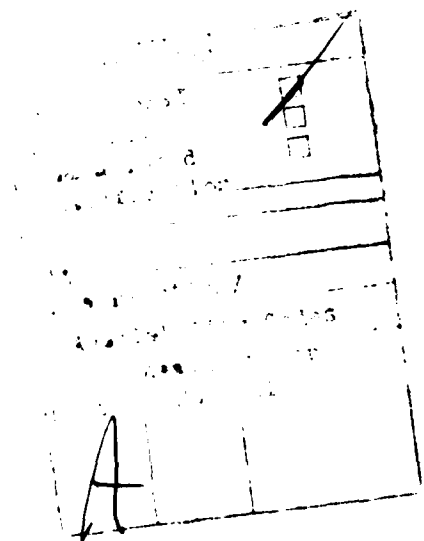
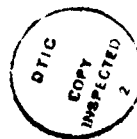
TABLE OF CONTENTS (Continued)

<u>CHAPTER</u>	<u>SECTION</u>	<u>DESCRIPTION</u>	<u>PAGE NO.</u>
6		CONCLUSIONS	78
APPENDIX		VERIFICATION OF THE POINT-MASS MODEL FOR THE DEFLECTION RATES	83
		ACKNOWLEDGEMENT	85
		REFERENCES	86



## LIST OF FIGURES

<u>FIGURE NO.</u>	<u>DESCRIPTION</u>	<u>PAGE NO.</u>
1	Illustration of the "raw" geoid	16
2	Illustration of the "observed" geoid together with the improvements due to orbital and tidal adjustment	17



## 1. INTRODUCTION

The short-arc model used at AFGL, the goals of which have included the computation of a relatively smooth surface approximating the geoid over the oceanic areas, is concerned with adjusting global satellite altimeter data in terms of a truncated set of spherical-harmonic (S.H.) potential coefficients. The altimeter data have been considered as the main source of observed quantities; gravity anomalies and other sources of geopotential information have been incorporated via the weighted S.H. coefficients. Six weighted state vector parameters per orbital arc are also included in the simultaneous least-squares process. One of the products of this adjustment is a revised set of S.H. coefficients which can be used to predict geoid undulations, gravity anomalies and other quantities related to the disturbing potential (e.g., deflections of the vertical) on a global scale. The main role of this adjustment is to provide a basis for a more detailed representation of the earth's gravity field to be carried out by means of subsequent adjustments.

The increasingly high quality of satellite altimeter measurements, in conjunction with the improvements in satellite ephemeris, calls for an adjustment model where at least some of the temporal variations in the ocean surface should be taken into account. The most important variations are those caused by the tide-generating forces of the moon and the sun. Of these, eleven long-period, diurnal, and semidiurnal tidal effects have been subjected to adjustment within the overall altimetric adjustment as described in [Blaha, 1982]. The initial (approximate) surface tide for the long-period constituents has been expressed through a relatively simple model based on the equilibrium tide with the earth deformation included. And the initial surface tide for

the diurnal and semidiurnal constituents has been based on a more realistic tidal model which takes into account the forces of friction and viscosity, the self-gravitation, the ocean loading effects, etc., and where the ocean tide has been expressed with the aid of spherical-harmonic tidal coefficients developed by Estes [1980]. The adjustable parameters modifying the initial tidal effects have been the amplitude corrections (for all the constituents) and the phase angle corrections (for the diurnal and semidiurnal constituents).

The global adjustment results in a "trend surface" approximating the geoid through the adjusted S.H. potential coefficients, and in the residuals representing the suppressed geoidal detail. Due to the relatively small amplitude of the geoidal residuals, the introduction of the spherical approximation in a subsequent adjustment is inconsequential. In the previous AFGL reports, e.g. [Blaha, 1979, 1980], one such adjustment has been developed in terms of point masses. In this approach, the location of the point masses is stipulated beforehand and only the point-mass (P.M.) magnitudes act as adjustable parameters. The role of these parameters is not merely to accommodate, in the least-squares sense, the residuals from the previous adjustment, but also to provide high-resolution predictions of the desired geophysical quantities.

The inclusion of the tidal parameters in the global adjustment results in an improved trend surface, as well as in improved residuals which otherwise would absorb the tidal variations. This, in turn, benefits the P.M. adjustment discussed above. The superimposition of the geoidal residuals on the adjusted trend surface results in new quantities, "observed" geoid undulations, which describe the surface called here the "observed" geoid.

The role of the tidal adjustment in improving the geoidal residuals and the corresponding "observed" geoid undulations will be discussed in Chapter 2 which will also outline the importance of these quantities in various geophysical tasks.

In the past, the P.M. parameters have been used in refining the geoidal surface -- and the knowledge of the earth's gravity field in general -- only over limited areas. This has been imputable to computer limitations, which are already felt when the number of P.M. parameters surpasses 200. In such adjustments all the point masses have been considered in conjunction with every observation point, i.e., all the P.M. parameters have been included in every observation equation. Although this is the proper approach from the theoretical standpoint, it makes a large-area or a global adjustment impractical in that exceedingly many small-area adjustments would have to be carried out in adjacent blocks in order to produce, for example, a geoidal map of a large ocean basin. Nonetheless, a simple elimination of point masses relatively far from an observation point could not alone alleviate this problem. The solution to this problem will be developed in Chapter 3 featuring a string of procedures assembled in what may be called a "modified Choleski algorithm".

Chapter 4, together with the Appendix, will be devoted to developing a new observational mode in terms of both the S.H. and P.M. parameters. This mode represents the rates in the deflections of the vertical along a given route. The adjustment model for the deflection rates has been inspired by the development of inertial instrumentation used with growing success in various geodetic tasks, notably in inertial navigation.

The adjustment models in terms of the P.M. parameters described in previous AFGL reports have been concerned with a single P.M. layer, i.e., with the point masses all located at the same depth. In Chapter 5 a concept of "twin" point masses located along the same normal to the earth's surface will be developed, corresponding to the notion of a double P.M. layer. All the observational modes treated previously will be given a twin P.M. formulation, including the deflection rates introduced above.

## 2. ROLE OF THE TIDAL ADJUSTMENT IN COMPUTING THE "OBSERVED" GEOID AS THE BASIS FOR A DETAILED GRAVITY FIELD REPRESENTATION

### 2.1 General Discussion

The parameters involved in the short-arc adjustment of satellite altimetry are divided into three groups: 1) corrections to the spherical-harmonic (S.H.) potential coefficients, 2) tidal parameters, and 3) corrections to the state vector (s.v.) components. The first group consists of 225 parameters in the case a (14,14) truncated S.H. model is used. The second group, absent in previous adjustments of satellite altimetry at AFGL, comprises two parameters per tidal constituent except for the long-period effects where this number is one per constituent. The first two groups are assigned permanent storage in the computer core. The third group consists of six s.v. parameters per (short) orbital arc. These parameters as well as the appropriate portions of normal equations are assigned reusable storage which is one of the main features of the short-arc algorithm described in detail in several AFGL reports and papers (for example, its brief review including several recent features can be found in [Blaha, 1981]). With the aid of this algorithm, the s.v. parameters are eliminated from the normal equations and are solved for later, after the solution of the first two groups of parameters, arc by arc.

At the outset it is useful to briefly recapitulate the highlights of the tidal adjustment as conceived in [Blaha, 1982], with emphasis on diurnal and semidiurnal constituents. It is based on a priori tidal information supplied by means of two (m,m) sets of S.H. tidal coefficients per constituent,

or  $2(m+1)^2$  coefficients. However, these coefficients are not being adjusted at all. Only two quantities, which are two specific functions of these coefficients, are adjustable for the chosen constituents: a parameter representing a proportional change in amplitude for the whole globe, and a parameter representing a change in phase angle for the whole globe. Accordingly, these parameters do not change with location or time. They also have a plausible physical meaning. In considering a global co-range map, the first would amount to changing the co-range number by the same proportion everywhere; and in considering a global co-tidal map, the second would amount to changing the phase angles by the same amount everywhere.

The above two parameters are not completely free to adjust but should be weighted according to their reliability. Clearly, since the tidal coefficients have been obtained by utilizing independent information subject to the solution of the Laplace Tidal Equations, their weight should not be zero. (These equations take into account the forces of friction and viscosity, the Coriolis force, the spatial distribution of depth, as well as the self-gravitation and the ocean loading effects as described in more detail in [Blaha, 1982], where heavy use was made of [Vaníček, 1980], [Estes, 1980], [Parke and Hendershott, 1980] and [Schwiderski, 1980].) And since the above two parameters represent certain linear combinations of the tidal coefficients, their weight should not be zero, either. Due to the lack of better information, the "one sigma" assigned for the independent weighting of these parameters in [Blaha, 1982] corresponded to 0.5 for the relative amplitude and  $10^0$  for the phase angle.

However, exceptions to any such weighting play an important role, depending on the satellite orbital characteristics. For example, care should be exercised when weighting the constituents  $K_1$ ,  $P_1$ ,  $S_2$  and  $K_2$  in conjunction with SEASAT altimeter data. As stated in [TOPEX, 1981], in this case the diurnal constituents  $K_1$  and  $P_1$  are aliased to a six-month and a constant constituent, respectively. The two semidiurnal constituents are similarly aliased to a six-month and a three-month constituent. Since the useful life span of SEASAT amounted to only about three months, most of these constituents cannot be properly resolved (even with aliasing taken into consideration), as is already the case with the semiannual constituent  $SSa$ . Accordingly, the a priori sigmas associated with the eight pertinent parameters (two parameters for each of the  $K_1$ ,  $P_1$ ,  $S_2$  and  $K_2$  constituents) have been substantially lowered in a recent tidal adjustment at AFGL.

A crucial part of any discussion involving a tidal adjustment is whether or not the tidal parameters are contaminated by geoidal and orbital errors. In the present case, the effect of the two tidal parameters on the modeled sea surface varies in time. For example, at a certain time when the phase is "zero" the effect of the amplitude and thus also of the amplitude change, whatever it may be, on the geocentric distance to the sea surface is zero. At another time, the effect is maximum. The geoid, by definition, is time invariant. This is true not only with respect to the geoidal features that are known and expressed by some means (e.g. via S.H. potential coefficients) but also with respect to the features not known or expressed, as well as to the features expressed erroneously. From the foregoing it follows that the present two-parameter solution should not be influenced, at least in theory, by the presence of geoidal errors.



A different question arises if one considers the observational noise, assumed random. If the sigma (standard error) of this noise is relatively large, many of the local tidal features may not be recoverable due to numerical difficulties. But the present two parameters pertain to all of the features, both large and small, in all of the oceans, associated with the given constituent. Thus, changes in these parameters affect the least-squares sum more than could be attributed to the comparable changes in the individual tidal coefficients and their various combinations (especially the combinations giving rise to small local tidal features). Accordingly, these parameters can be resolved better than other tidal quantities could. However, a good quality in the solution can be achieved only if these tidal parameters are sufficiently independent of the systematic errors in the adjustment. The independence with regard to geoidal errors has been shown in the preceding paragraph.

The effect of orbital errors on the recoverability of tidal parameters causes, in general, the greatest concern. In this context, the reference heavily relied upon will be [Estes, 1980]. Its opening statements acknowledge that the efforts to extract ocean tide information from satellite altimetry data have been largely unsuccessful, mostly due to errors in the orbit determination. In particular, it states:

"The tidal frequencies are well determined from astronomical considerations, and computer simulations by Zetler and Maul (1971) and by Won et al. (1977) strongly indicate the possibility of recovering the principal tides with widely spaced time sampling using this type of data. However, these simulations have treated measurement noise and random orbit error, but have not considered the aliasing effects of systematic orbit error, which over local regions can resemble a tide signal."

At this point one notices the term "local regions", which can be contrasted to the global character of the above two parameters. The same reference further states that unmodeled systematic errors are significant and must be considered in the analysis for tidal structure from satellite altimeter data. Here the term "tidal structure" clearly applies to all of the features pertaining to a given tidal constituent, not merely to the amplitude and phase changes made uniform for the whole globe.

The main result of the above reference is expressed on page 92:

"The present results demonstrate that with adequate modeling of the ephemeris errors to reduce the aliasing of the tides, simultaneous estimation of the tide model and radial orbit error model parameters will accurately recover the principal tidal constituents."

It will be shown that the present model is different from Estes' (and from that of the other investigators as quoted above) and that it does not require model parameters for systematic orbital errors. The key consideration lies in its scope, in that it does not seek to recover the entire tidal constituent as described by  $2(m+1)^2$  S.H. tidal coefficients. Instead, it attempts to recover only two parameters which, furthermore, are weighted.

The concern addressed in [Estes, 1980] is the separability of the orbit error and the tide (see p.76). But the term "tide" implies all of the S.H. tidal coefficients. This is clear, for example, from p.83 where the total number of adjustment parameters is given as

$$220 \times NC + 50 \times (2NP + IB + IS).$$

The first term pertains to all the S.H. tidal coefficients for all the tidal

constituents. The second term then includes the model parameters for systematic orbital errors on all of the 50 satellite arcs considered. One further notices the statement on page 81:

"In the least-squares recovery for the model parameters, the a priori values of the expansion coefficients are set to zero."

At this point, the S.H. coefficients in [Estes, 1980] are seen as:

- a) not known a priori,
- b) given zero values a priori,
- c) given zero weight a priori,
- d) all subject to adjustment.

On the other hand, the S.H. tidal coefficients in the present adjustment are

- a) known a priori,
- b) given their a priori values obtained from an independent source,
- c) not considered for weighting, etc., because they are not adjustable parameters individually; in particular,
- d) only two special combinations are subject to adjustment, they are assigned two parameters and these are attributed weights according to their reliability.

Except for the two special kinds of changes as embodied by the above two parameters, the whole configuration (in space and time) of the tidal constituent in question is adopted completely from the a priori information. Clearly, if one wanted to resolve all of the S.H. tidal

coefficients, one would be faced with the necessity of modeling the orbital errors as demonstrated by Estes [1980]. In circumventing such a task, the present model represents a limited adjustment which can still improve the tidal knowledge, reduce the residuals and, perhaps, indicate deficiencies in the a priori tidal information by using satellite altimetry as an independent source. The term "limited adjustment" should be understood a) as incorporating only two parameters per constituent, and b) as considering even these parameters weighted. Due to the weighting, unless there exists a strong inconsistency between the altimetry and the a priori tidal information, the corrections to these parameters are expected to be relatively small.

The characteristics of the present model are further elucidated if one recalls that a tidal constituent is described by several properties, such as the number and locations of amphidromic points, the shape of the co-phase lines (emanating from the above points) anywhere on the globe, the shape of the co-range lines anywhere on the globe, etc. These properties are described by the a priori information considered here to be the S.H. tidal coefficients. If these coefficients were subject to adjustment, changes in any or all of them would bring changes to any or all of the above properties and vice versa. Thus, if altimeter data were contaminated by systematic errors over a given area, the coefficients resolved in an adjustment would in general all be affected to a certain extent. This, in turn, would affect any or all of the tidal properties in that area.

However, the present tidal model allows for only two very special changes in two specific properties: 1) the change in co-range numbers by the same proportion over the whole globe and 2) the change in co-phase

numbers by the same amount over the whole globe, out of an infinite number of all possible global and local changes. As it has just been indicated, the local properties respond to systematic orbital changes in various areas and during various time periods. But only some very special systematic errors in the orbit, present all over the globe all of the time, could introduce changes in the above two special properties. Even though systematic orbital errors exist they tend to "average out" in space and time, especially periodic errors. One could conclude these heuristic arguments by stating that if any properties of a tidal constituent are insensitive to such systematic orbital errors, it is those representing the very special global shifts in the co-range and co-phase lines described by the two tidal parameters in the present adjustment model.

## 2.2 Effect of Tidal Modeling on the SEASAT Altimeter Adjustment

During recent data reductions at AFGL, some 6,700 arcs of SEASAT altimetry have been adjusted in the short-arc mode, where the arcs' durations have been seven minutes or less. This adjustment has yielded for  $M_2$  a 22% reduction in amplitude and a  $0.7^\circ$  change in phase angle as given by the initial set of (12,12) S.H. tidal coefficients supplied by Estes [1980]. Such small changes indicate a realistic model for this constituent whose effect is twice to several times greater than the effect of the other tidal constituents. The permanent tide is an exception to this statement, but its effect is still lower than that of  $M_2$ ; mathematically, it can be related to the earth's flattening.

The inclusion of the tidal effects into the adjustment has resulted in slight overall reductions in the size of the residuals and the related quantities, as compared to the original adjustment where these effects were not considered. But to better understand the relative smallness of these reductions the difference between the "tide" (denoted by the index "t") and the "no tide" (denoted by the index "nt") results are presented, where  $v$  is the residual and  $\Delta u$  is the "up" correction to the s.v. components:

$$\Delta v = v_t - v_{nt} ,$$

$$\Delta(\Delta u) = \Delta u_t - \Delta u_{nt} .$$

From randomly distributed satellite passes all over the globe, it has been found that the average  $\Delta v$  and average  $\Delta(\Delta u)$  are nearly zero; their RMS values

have been computed as

$$\text{RMS } (\Delta v) = 0.047\text{m} ,$$

$$\text{RMS} [ \Delta(\Delta u) ] = 0.187\text{m} .$$

Using a majority of the adjusted arcs,  $v_t$  and  $v_{nt}$  have been found to have a nearly zero average value; further,

$$\text{RMS } (v_t) = 1.733\text{m} , \quad \text{RMS } (v_{nt}) = 1.734\text{m} .$$

Clearly, the RMS improvement in  $v_t$  as compared to values  $v_{nt}$  is very small because  $\text{RMS } (\Delta v)$ , although itself reaching 5cm, is small by comparison. In fact, it turns out that  $1.733^2 + 0.047^2 \approx 1.734^2$ , which could be given a rough interpretation where  $\Delta v$  could represent random errors attached to  $v_t$  in order to yield  $v_{nt}$  in a stochastic process on a sphere. A reduction in  $\text{RMS } (\Delta u)$  is also very small, represented by

$$\text{RMS } (\Delta u_t) = 1.869\text{m} , \quad \text{RMS } (\Delta u_{nt}) = 1.875\text{m} .$$

In analogy to the above,  $\text{RMS } [\Delta(\Delta u)]$  is small when compared to these values and  $\Delta(\Delta u)$  can be given an interpretation similar to that for  $\Delta v$ . The RMS value of 1.869m (and also 1.875m) in the "up" correction to the state vectors compares very well with the a priori sigma of 1.6m associated with the NSWG precise ephemeris used.

One of the most important results of SEASAT altimetry and tidal adjustment are the "observed" geoid undulations, denoted  $N_{\text{og}}$ , describing the "observed" geoid. The quotes are used to indicate that certain

improvements have taken place in relation to more directly observed undulations, called here the "raw" geoid undulations. The latter, denoted  $N_{"r"}$ , describe the "raw" geoid illustrated in Figure 1. A "raw" geoid undulation is given essentially as the initial radial distance (from the geocenter) to the satellite, minus the radial distance to the altimeter foot-point on the ellipsoid, minus the altimeter measurement, plus the small correction "d", due to the earth's flattening, mentioned e.g. in Section 4.1 of [Blaha, 1982]. The "observed" geoid, depicted in Figure 2, can be constructed from the "raw" geoid through two refinements, 1) by utilizing the adjusted (rather than initial) s.v. components and 2) by considering the adjusted tidal effects.

The direct representation of the "observed" geoid is made through the first equation in Figure 2,

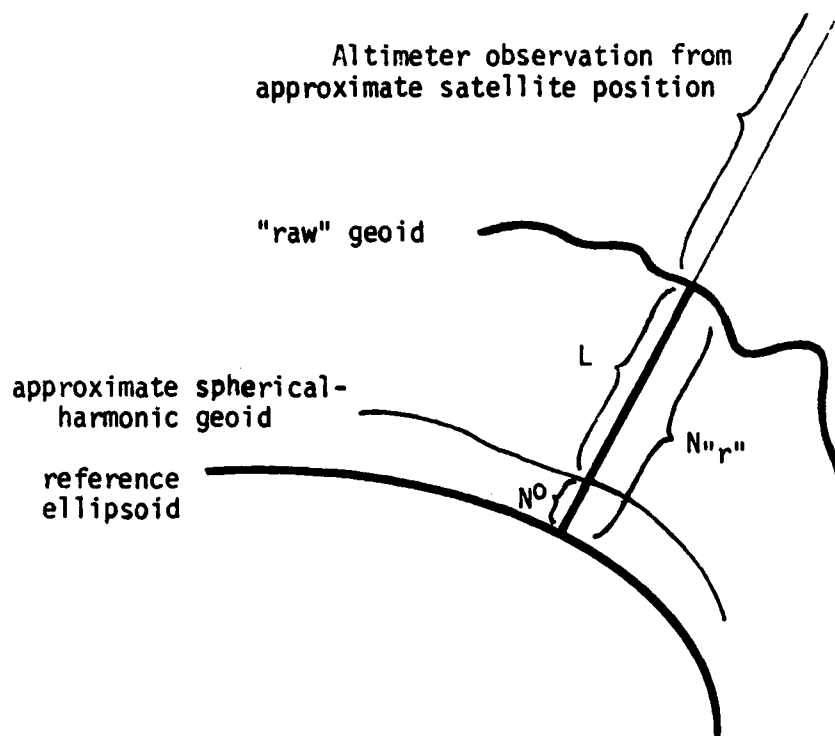
$$N_{"o"} = N^a + v ,$$

where  $N^a$  is the adjusted geoid undulation computed from the adjusted set of S.H. potential coefficients and  $v$  is the residual as introduced earlier. The representation displaying the difference between the "observed" and the "raw" geoids is given in the second equation of the same figure as

$$N_{"o"} = N_{"r"} - i_1 - i_2 ,$$

where  $-i_1$  is the improvement due to the orbital adjustment (i.e., adjustment of the s.v. components) and  $-i_2$  is the improvement due to the adjusted tidal effects. At a mid-arc epoch the quantity  $-i_1$  coincides with the "up" correction whose characteristics have been already discussed. The RMS of  $-i_2$



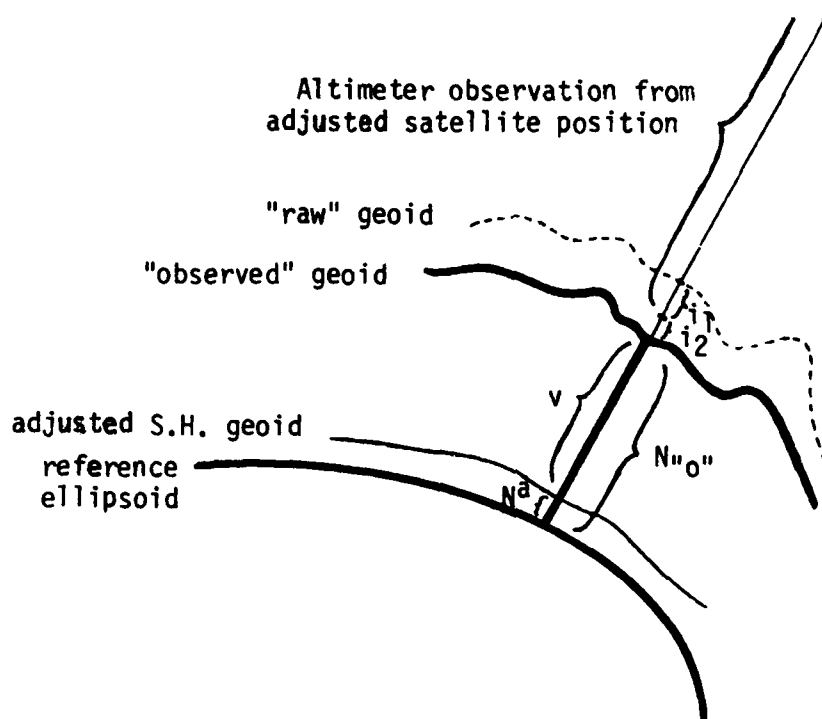


$$N_{r''} = N^0 + L \quad \dots \quad N_{r''} = \text{"raw" geoid undulation}$$

$N^0$  = geoid undulation correspond-  
ing to approximate spherical-  
harmonic potential coefficients

$L$  = constant term of altimeter  
observation equation in the  
spherical-harmonic model

Figure 1  
Illustration of the "raw" geoid



$$N''_0 = N^a + v \quad \dots \quad N''_0 = \text{"observed" geoid undulation}$$

$N^a$  = geoid undulation corresponding to  
adjusted S.H. potential coefficients

$v$  = residual in the S.H. model

$$N''_0 = N''_r - i_1 - i_2 \quad \dots \quad -i_1 = \text{improvement due to orbital adjustment}$$

$-i_2$  = improvement due to  
tidal adjustment

Figure 2

Illustration of the "observed" geoid together with the  
improvements due to orbital and tidal adjustment

has been computed from the randomly distributed arcs mentioned earlier as 29cm, which is indeed a realistic value for open ocean.

The improvements in  $N_{"0"}$  due to the tidal adjustment can be assessed by comparing the corresponding results with the non-tidal adjustment according to

$$\Delta N_{"0"} = \Delta N^a + \Delta v ,$$

where  $\Delta v$  was already defined and where

$$\Delta N^a = N_t^a - N_{nt}^a ,$$

$$\Delta N_{"0"} = N_{"0"}^t - N_{"0"}^{nt} .$$

From the same arcs as before, the RMS values have been computed as

$$\text{RMS} (\Delta N^a) = 0.111\text{m} ,$$

$$\text{RMS} (\Delta N_{"0"}) = 0.121\text{m} .$$

The improvements in  $N^a$  and, more importantly, in  $N_{"0"}$  due to the tidal adjustment are thus seen to be at the decimeter level.

In the past, the "observed" geoid undulations along the SEASAT passes were useful in a study of ocean-bottom phenomena, especially the bathymetry. But the benefits of the "observed" geoid do not end there. For example, after having a smooth "trend surface" (corresponding to a 14,14 S.H. model or otherwise) removed from this geoid, the resulting differenced undulations can serve in expressing the geoidal surface to a desired resolution, whether on a regional or a global scale.

### 2.3 Summary and Assessment of the "Observed" Geoid

The adjustment model of satellite altimetry presented herein has been based on the short-arc algorithm. In addition to the newly introduced tidal parameters the adjustment model includes a set of low degree and order spherical-harmonic potential coefficients, typically a (14,14) set, and a set of orbital parameters comprising six state vector components per orbital arc. All these parameters are subject to a simultaneous least-squares adjustment. In earlier as well as recent adjustments, the potential coefficients and the state vector components have been weighted according to their reliability specified at the source (GEM 10 coefficients, NSWG precise ephemeris). The weights for the tidal parameters have been introduced in [Blaha, 1982] as corresponding to the a priori sigma of 1 (long-period constituents) or 0.5 (diurnal and semidiurnal constituents) for the relative amplitudes, and to the a priori sigma of  $10^0$  for the phase angles. However, the weights have been substantially increased in the case of  $K_1$ ,  $P_1$ ,  $S_2$  and  $K_2$  constituents which cannot be properly resolved by SEASAT altimetry and would otherwise be aliased into constituents of lower frequencies.

The adjustment including the tidal effects represents an improvement over an earlier non-tidal adjustment of altimeter observations. The differences between the two kinds of adjustments translate into about 11cm RMS for the adjusted geoid (computed from the adjusted coefficients), 5cm RMS for the residuals, 19cm RMS for the "up" component of the state vectors and 12cm RMS for the "observed" geoid. The latter is obtained by adding the residuals to the corresponding adjusted geoid undulations, and is equivalent to the directly observed "raw" geoid improved through the adjustment

corrections to the state vectors and through the adjusted tidal effects. Since the "observed" geoid plays a major role in a detailed determination of the earth's gravity field, an improvement at a decimeter level can be significant.

The features offered by the short-arc altimetry adjustment including the tidal effects are now briefly summarized:

- The adjustment is global in nature and is capable of discerning important tidal effects.
- The inclusion of the tidal effects has lead to a 5cm RMS improvement in the residuals (as opposed to a "non-tidal" adjustment) with the consequence of a slight reduction in the overall magnitude of the residuals.
- A similar conclusion has been reached for the "up" corrections to the state vectors (the improvement has been 19cm RMS), whose overall RMS value of 1.87m compares very well with the a priori sigma of 1.6m.
- The improvements in the adjusted geoid (computed from the adjusted spherical-harmonic potential coefficients) and in the "observed" geoid have amounted to 11cm and 12cm RMS, respectively.
- The "observed" geoid and the corresponding residuals can play an important role in detecting and studying a variety of ocean-bottom phenomena.
- The "observed" geoid can serve in refining the global oceanic geoid via various prediction techniques. One such technique uses the point-mass parameters as explained in previous AFGL reports as well

as in Chapters 3 and 5 herein. As an example of another technique, the "observed" geoid can be used to produce a high degree and order set of spherical-harmonic potential coefficients via integral formulas, which can then serve in predicting geoid undulations and other geophysical quantities related to the disturbing potential (e.g., gravity anomalies, deflections of the vertical, etc.).

- One can conclude that in taking advantage of the adjusted state vectors and the adjusted tidal effects, and of the high-resolution residuals at the same time, the "observed" geoid leads to improvements in a detailed representation of the earth's gravity field. As one example of using these high-resolution residuals in an independent approach, techniques are being developed at AFGL to compute gravity anomalies from the "observed" geoid or the corresponding residuals along certain ocean trench areas, which have already shown a good agreement with the ground truth.

### 3. LARGE AREA ADJUSTMENT USING THE POINT MASS PARAMETERS

#### 3.1 Notes on the Strategy in Choosing the Depth-Side Ratio of Point Masses

In one of the original reports on a point-mass (P.M.) adjustment, [Needham, 1970] suggested the depth/side ratio for point masses,  $d/s$ , as 0.8/1. That study concentrated to a great extent on gravity anomalies. In the AFGL report [Blaha, 1979], both gravity anomalies and geoid undulations were taken into consideration in the computer simulations which eventually lead to the recommendation that the above ratio be doubled, in the sense  $d/s = 1.6/1$ . However, due to the computer core limitations, both the simulated data and the spherical-harmonic (S.H.) coefficients recovered from the first adjustment corresponded to only a very low degree and order S.H. expansion. In a typical case, "errorless" data were generated with a given (10,10) set and the first (global) S.H. adjustment was performed in terms of a (6,6) set. This means that the P.M. parameters were to accommodate the residuals from the first adjustment, which only contained the gravity field information within (7,7) to (10,10) truncation.

At the present, the first adjustment alone corresponds to a (14, 14) set of S.H. potential coefficients and the P.M. parameters (i.e., P.M. magnitudes) are distributed typically in a  $2^0 \times 2^0$  equilateral grid which serves to accommodate the residuals within an up to about (90,90) equivalent truncated set. It is clear that the P.M. depth should be related to the information contained within (15,15) to (90,90) truncated sets, whereas the simulations, as stated above, could only take into consideration (7,7) to (10,10) sets. For this reason the ratio 1.6/1 is not considered final.

Another motivation for re-examining the ratio  $d/s = 1.6/1$  is practical in nature. If all the P.M. parameters were included in the formation of every observation equation as was the case with the above computer simulations, the computer run-time would be exceedingly high, especially if a detailed, large-scale adjustment of the oceanic geoid were required. Furthermore, the computer storage difficulties would be almost insurmountable without the use of an algorithm tailored for a banded structure of normal equations. Such an algorithm, described in the next section, stipulates that beyond a certain spherical cap centered on an observation point (or, equivalently, beyond a certain cut-off distance) the P.M. parameters are ignored in the pertinent observation equation. This introduces approximations in the adjustment model which, however, are inconsequential if the effect of the neglected P.M. parameters on the modeled value at the observation point is very small compared to the effect of the point masses located in the vicinity of this point. In using a special arrangement of the P.M. parameters, the above cut-off distance represents a transition from a full matrix of normal equations (N) to a banded matrix. The next paragraph further elaborates on this property.

In a P.M. adjustment model the correlation between the parameters decreases as the distance between the corresponding point masses grows larger. In using a special design for grouping the parameters, most of the off-diagonal elements in the matrix N can be made very small (in the sense that the further from the main diagonal, the smaller the elements become). Without a significant loss of accuracy some of these elements can be set to zero, resulting essentially in a banded system of normal equations. In practice, this task can be accomplished at the level of observation



equations, in conjunction with the cut-off distance described above. The resulting system can then be resolved with a great efficiency by a modified Choleski algorithm. Such an algorithm allows for the inclusion of many more P.M. parameters in the adjustment, perhaps ten-fold, than would otherwise be possible due to the computer storage and run-time limitations. This approach can be used in conjunction with both the single and the twin point masses (the latter are described in Chapter 5). As a result of the above modeling approximation, a detailed resolution of the geoidal surface and the earth's gravity field is made possible on a large, or even global, scale.

The efficiency of the modified Choleski algorithm increases, both from the run-time and computer core standpoints, if the bandwidth in the matrix  $N$  decreases. In considering a suitable arrangement of the parameters according to the P.M. locations, the bandwidth is linked directly to the size of the spherical cap, in the sense that a smaller cut-off distance results most often in a smaller bandwidth. But the cut-off distance can be reduced without unduly compromising the rigor of the solution only if the "kernel" function, representing the effect of a point mass on the modeled value, decreases sufficiently with distance. When examining the relative values of this function at various  $n$ -multiples of the P.M. separation  $s$ , one could be guided by the following very approximate classifications:

40% - 50% effect remains ..... cut-off decision is marginal,  
20% - 40% effect remains ..... cut-off decision is sufficient,  
under 20% effect remains ..... cut-off decision is more than  
sufficient.

Clearly, a shallower point mass results in a kernel function which decreases more rapidly with increasing distance. If the ratio  $d/s = 1.6/1$  were used, the cut-off decision would have to be made in favor of  $n=3$  or  $n=4$  with regard to some of the observational modes described in [Blaha, 1980], especially the geoid undulations. Being derived directly from satellite altimetry, the geoid undulations represent the most important mode in the P.M. adjustment. With the cut-off distance of 3s or 4s the computer requirements would still be unrealistically high for a geoidal adjustment in a large ocean basin such as the Indian Ocean, etc. However, if  $d/s$  is lowered to the original ratio of  $0.8/1$ , the same approximation level is compatible with the cut-off distance of only 1.5s or 2s. One could lower this ratio even further but it might not be desirable for other reasons (in [Needham, 1970], this ratio represented a close relationship between the P.M. blocks and the gravity anomaly blocks). Be that as it may, the  $0.8/1$  ratio adopted in conjunction with the cut-off distance of 1.5s appears satisfactory for the purpose at hand, as is illustrated next.

In view of the new ratio  $d/s = 0.8/1$ , the kernel functions for the five observational modes analysed in [Blaha, 1980] must be re-examined. The value  $s$  of the P.M. separation now corresponds to 445 km ( $4^\circ$  in arc measure), whereas the value of  $d$  remains at 350 km. The theoretical outcome of such an analysis is not tied to a specific P.M. separation (for example,  $2^\circ$  in arc measure could be used as well, etc.) because one is interested merely in the relative P.M. effect as a function of  $n$ . The results presented in the above reference, computed for a point mass whose magnitude is a  $10^{-6}$ th part of the earth's mass, are modified as follows:

### Geoid undulations

n = 0	..... 116 m (100%)	n = 1.5	..... 55.2 m (47.6%)
n = 0.5	..... 98.9 m (85.3%)	n = 2	..... 43.6 m (37.6%)
n = 1	..... 73.1 m (63.0%)	n = 2.5	..... 35.8 m (30.9%)

### Gravity anomalies

n = 0	..... 290 mgal (100%)	n = 1	..... 62.0 mgal (21.4%)
n = 0.5	..... 172 mgal (59.3%)	n = 1.5	..... 21.2 mgal ( 7.3%)

### Deflections of the vertical

n = 0	..... 0.0" ( 0%)	n = 1	..... 20.5" (79.8%)
n = 0.25	..... 18.0" (70.0%)	n = 1.5	..... 13.2" (51.4%)
n = 0.5	..... 25.4" (98.8%)	n = 2	..... 8.7" (33.9%)
n = 0.57	..... 25.7" (100%)	n = 2.5	..... 6.0" (23.3%)
		n = 3	..... 4.4" (17.1%)

### Horizontal gradients of gravity disturbance

n = 0	..... 0.00 E ( 0%)	n = 0.5	..... 7.54 E (97.3%)
n = 0.25	..... 6.68 E (86.2%)	n = 1	..... 3.44 E (44.4%)
n = 0.45	..... 7.75 E (100%)	n = 1.5	..... 1.33 E (17.2%)
		n = 2	..... 0.58 E ( 7.5%)

### Vertical gradients of gravity disturbance

n = 0	..... 18.59 E (100%)	n = 1	..... 0.67 E ( 3.6%)
n = 0.5	..... 6.97 E (37.5%)	n = 1.5	..... -0.19 E (-1.0%)

As it appears from the above, the cut-off distance at  $n=1.5$  is more than sufficient for all the observational modes except geoid undulations and deflections of the vertical, for which it can be termed marginal. However, due to practical considerations (especially the bandwidth) this distance is adopted in all cases. If the ratio  $d/s=1.6/1$  had been used for undulations,  $n=1.5$  would have corresponded to the effect of about 75%. This would have lowered the rigor of the least-squares adjustment, increased the residuals, etc. A test adjustment for a limited area in the North Atlantic has confirmed that with the same cut-off distance of  $1.5s$ , the  $0.8/1$  ratio leads to a very slightly lower RMS residual than the  $1.6/1$  ratio. In particular, the  $1.6/1$  ratio has produced a 1.59 m RMS residual, the  $1.2/1$  ratio has produced a 1.58 m RMS residual, and the  $0.8/1$  ratio has produced a 1.56 m RMS residual using the same data of SEASAT altimetry. The computer simulations mentioned earlier yielded a different outcome (a higher ratio resulted in a lower RMS residual) due, to a great extent, to the theoretical treatment in which the cut-off distance was infinite, and also due to a low level of geoidal variation as implied by the generated data.

### 3.2 Point-Mass Algorithm for a Banded System of Normal Equations

The cornerstone of the present development is an application of the Choleski algorithm to a large scale geoid determination from satellite altimetry. The reason for using this algorithm is that it lends itself well to an accurate and efficient solution of nonsingular (therefore, positive-definite) systems of normal equations, especially banded systems. The latter are characterized by a great number of zero elements in the matrix of normal equations ( $N$ ), located outside of a central band. However, before arriving at a banded system a reformulation of the least-squares problem often has to take place.

In the present context one strives for the smallest possible number of parameters, i.e., point-mass (P.M.) magnitudes, to be involved in one observation equation. But this is only a part of the task, and an easy part at that; the number of P.M. in such an equation can be made almost arbitrarily small by decreasing the dimension of a spherical cap centered on an observation point beyond which the P.M. are ignored. Clearly, this represents a simplification which should not be overused because the rigor of the solution could suffer. Besides, if the numbering of the parameters were done in a haphazard way, the span between the P.M. with the lowest number and the one with the highest number in the observation equation could still be great and thus the bandwidth would be large. There might be a great number of zeros within the band, but this represents no advantage since such zeros cannot benefit the algorithm. The main task, therefore, is that of a proper design of the P.M. network and of P.M. numbering.

The most natural distribution of P.M. is that of an equilateral grid, in that it does not favor any particular region and the resolution is uniform. A basic example of an equilateral grid of P.M. appears below. The parameters are numbered in columns (N-S direction) because it is anticipated that the longitudinal extent of the grid will be greater than its extent in latitude and thus a smaller span will be involved with one observation point. If the ocean basin is too great for a strip-like grid of P.M. to cover it, overlapping grids can eventually result in a uniform geoidal representation of this basin and, indeed, of all of the world's oceans. The observations for each strip would have to overlap as well, for the sake of a smooth transition of geoid contours, etc., between the strips. As a practical matter, several adjacent strips may be present in one adjustment. In a number of cases along the borderlines, two P.M. parameters will be assigned the same physical location, one P.M. belonging to the upper strip and the other one, with a much higher rank number, belonging to the lower strip. Because of the rank disparity the algorithm will treat these double P.M. completely independently. To assure continuity between the strips (predictions, contour lines), each such location could be assigned one final parameter represented by the average of the two P.M. magnitudes. However, this would imply the renumbering of the parameters before the predictions could begin. The simplest solution to this problem, yielding exactly the same results, is to leave the numbering unchanged and to divide the magnitude of each double P.M. by two.

1	$n_1+1$	$2n_1+1$	$3n_1+1$				
x	x	x	x	x	x	x	...
2	$n_1+2$	$2n_1+2$					
x	x	x	x	x			
3	$n_1+3$	$2n_1+3$					
x	x	x	x	x			
4							
x	x	x	x	x			
⋮							
$n_1$	$2n_1$	$3n_1$					
x	x	x					

In the illustration above the "x" represent the P.M. and "0" is the observation point whose observation equation is being formed. If  $s$  is the separation of neighboring P.M. and if the radius around 0 beyond which the P.M. are ignored in this equation is just under  $1.5s$ , the span of the P.M. involved is  $2n_1+3$ , the present case comprising the P.M. numbered 1 as the lowest number and  $2n_1+3$  as the highest number. There are, of course, many P.M. in between which are omitted from this observation equation (e.g. those numbered 4, 5, ...,  $n_1+4$ , etc.). The number of "rows" of P.M. is denoted as  $n_1$  and the number of "columns" is denoted as  $n_2$ . The total number of parameters ( $n$ ) in such a grid is then

$$n = n_1 n_2 . \quad (3.1)$$

On the other hand, the bandwidth ( $b$ ) in the matrix of normal equations under

the circumstances illustrated above is

$$b = 2n_1 + 3 . \quad (3.2)$$

The bandwidth is defined as the largest number of elements in any row of  $N$ , starting with the diagonal element, beyond which all the elements are zeros. It is given by the largest span in the matrix of observation equations (A) which, in the present case, is  $2n_1 + 3$ .

The physical limitations to the geoidal representation, both in the extent of the area and in the resolution capabilities, are given by the number of elements in  $N$  which have to be stored. In the case of no bandwidth implementation this storage space ( $S$ ) is

$$S = n(n+1)/2 \quad (3.3)$$

elements, provided only the upper triangular portion of  $N$  is stored (for the whole matrix  $N$  this storage would be  $n^2$ ). On the other hand, if only the bandwidth is stored, starting with the diagonal elements, the storage space ( $S'$ ) becomes

$$S' = bn . \quad (3.4)$$

This storage is actually conservative, in the sense that the band has been extended by  $(b-1)b/2$  elements (zeros) in order to conform to a rectangular form facilitating the implementation of a modified Choleski algorithm.



In considering (3.1)-(3.4), the storage savings associated with the bandwidth approach can be expressed as

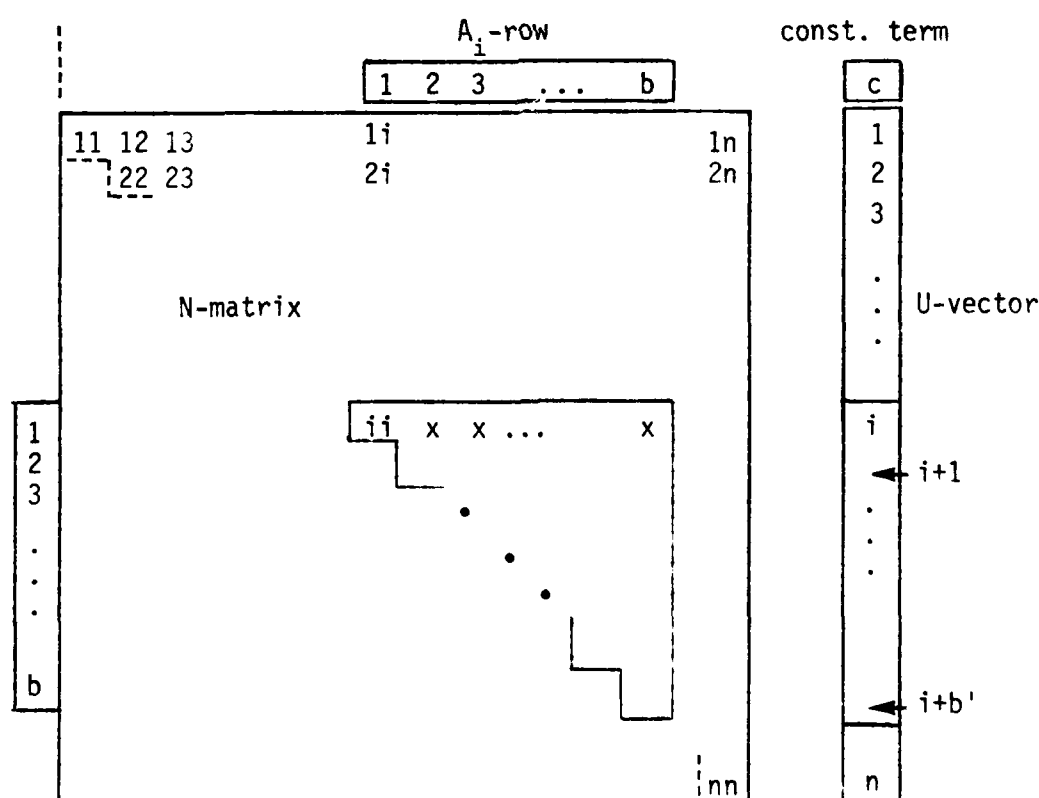
$$S'/S = 4(n + 3/2)/(n+1) \approx 4/n_2. \quad (3.5)$$

The approximate relation in (3.5) can be adopted for a reasonably large  $n_1$ , perhaps 20 or more. It shows that with an increasing number of "columns" of P.M. the storage economies grow. Thus if  $n_2=100$ , the economies should improve about 25-fold. This can be illustrated with an example where  $n_1=20$ ,  $n_2=100$  and thus  $n=2000$ . The approximate value of  $S'/S$  was just shown to be  $1/25$  while the exact value is  $1/23.3$ . In particular,  $S = 2,001,000$  and  $S' = 86,000$ . Thus one can see the beneficial effect of the bandwidth approach not only from the economy point of view in itself but, especially, because it allows an adjustment on a large scale which would otherwise be unthinkable.

Due to possible irregularities in the P.M. grid the band can initially be larger than the final  $b$ . If the former is adopted in the algorithm, one or more of its first rows could contain only zeros. This would detract from possible economies but, most of all, it would make the algorithm break down, as if  $N$  were singular. For this reason it is useful to search for zero rows in the band, eliminate them and arrive at a final bandwidth. The original bandwidth can be denoted as  $\max b$  and it can be stipulated as  $2n_1+3$  or perhaps even higher. The final bandwidth is denoted as  $b$ ; in most cases it will be the same as  $\max b$ , but its implementation is a simple matter well worth the effort.

Next, the formation of the special matrix  $\tilde{T}$  will be addressed, based on one row ( $A_1$ -row) of  $A$ . The transposition of this row results in a column

which, when post-multiplied by  $A_i$ -row fills the matrix  $N$  (mostly with zeros). When this operation is performed with all the other rows corresponding to all the other observations, where the contributions are added algebraically, the final matrix  $N$  is formed. All the  $A_i$ -rows are assumed to have been scaled by the a priori sigma of the observations considered mutually independent so that weighting need not be considered. The right-hand side (column vector  $U$ ) of normal equations is formed in a similar fashion, except that the transposed  $A_i$ -row is post-multiplied by the corresponding constant term  $c$  (an element of  $L^b-L^0$  in adjustment notations). Due to the span considerations, the  $A_i$ -row will have only  $b$  elements (actually, one would start with max  $b$  elements and, at the end, "squeeze out" the zero rows from  $\tilde{T}$ , if any; but it is not difficult to imagine the following scheme apply with max  $b$  replacing  $b$ ).



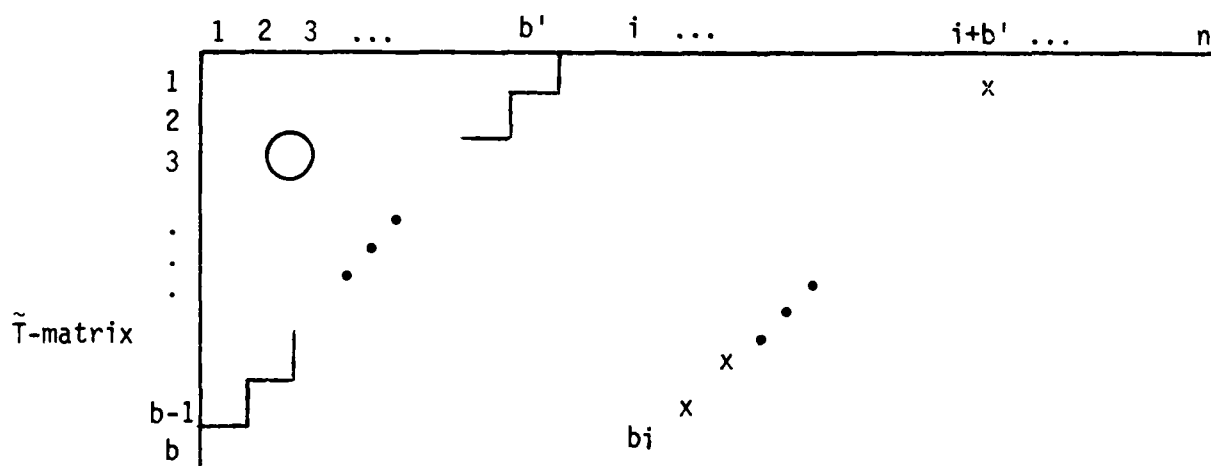
Depicted above is the formation of  $N$  with the aid of one  $A_i$ -row; the other such rows would perform a similar role as already explained. The  $U$ -vector is also illustrated. The zig-zagging line indicates the upper-triangular portion of  $N$  which is of interest. The first element in  $A_i$ -row corresponds to the column  $i$  in  $N$ . In the computer, the rank number of the P.M.  $i$  is retained for addressing in  $N$  and the  $A_i$ -row's addressing begins with 1. It ends with  $b$  which, in  $N$ , corresponds to  $i+b'$ , where

$$b' = b - 1. \quad (3.6)$$

The important property of the algorithm being developed is that the  $\tilde{T}$  matrix will not comprise the whole upper triangular portion of  $N$ , but only its  $b$ -band (the zeros outside the band are simply disregarded). To facilitate the addressing,  $\tilde{T}$  is enlarged to include the (nonexisting) elements in  $N$  which would fill a triangular matrix extending from the upper-left corner of the latter. Such a triangular matrix would continue the border of  $N$  along the dashed line for the length of  $b'$  elements; its base would also have  $b'$  elements so that the total number of elements in it would be  $(b-1)b/2$ . If this matrix is adjoined to the  $\tilde{T}$ -portion of  $N$ , the resulting array  $\tilde{T}$  will have  $b$  "jagged" rows and  $n$  columns. This array is finally "straightened out" to form a rectangular array which is the desired matrix  $\tilde{T}$  with  $b$  rows and  $n$  columns.

The rows in  $N$  are represented by ascending diagonals in  $\tilde{T}$  as indicated below, where the elements "x" correspond to the elements so denoted in the last illustration. The  $(b-1)b/2$  nonexisting elements of  $N$  discussed

above are represented by zeros in  $\tilde{T}$ . Clearly, the diagonal elements in  $N$  occupy the last row in  $\tilde{T}$ . Thus the "ii" element in  $N$  corresponds to the "bi" element in  $\tilde{T}$  as illustrated.



The matrix  $\tilde{T}$  is not formed from  $N$  (this would entail a large storage) but directly from the  $A_i$ -rows. The element  $ii$  in  $N$  has the location  $bi$  in  $\tilde{T}$ ; the element next to the right in  $N$ ,  $i, (i+1)$ , has the location  $(b-1), (i+1)$  in  $\tilde{T}$ , followed by  $(b-2), (i+2)$ , etc. The last element within the band  $b$  in that row of  $N$  has the location  $1, (i+b')$  in  $\tilde{T}$ . Thus the matrix  $N$  has served only mentally, without any computer core requirements. All the "ascending diagonals" in  $\tilde{T}$  are formed according to the same principle, except that the last diagonals end at the column  $n$  and do not reach the first row of  $\tilde{T}$  (they have fewer elements than  $b$ ). The vector  $U$  is not modified in conjunction with the formation of  $\tilde{T}$ . Mathematically, the above principle of addressing can be symbolized as follows:

$$i, i \rightarrow b, i; \quad i = 1, 2, \dots, n \quad (3.7a)$$

$$i, j \rightarrow b-(j-i), j; \quad j = i+1, i+2, \dots, n. \quad (3.7b)$$

Next, the modified Choleski algorithm will be developed to treat the problem at hand, in conjunction with the above matrix  $\tilde{T}$ . With the customary adjustment notations the least-squares solution of the vector of  $n$  (unknown) parameters,  $X$ , is expressed as

$$X = N^{-1}U,$$

where

$$N = A^T A, \quad U = A^T (L^b - L^o),$$

and where  $L^b$  is the vector of observations while  $L^o$  is the vector of the corresponding initial values. As mentioned earlier, the weighting of observations need not be applied here. The variance-covariance matrix ( $\Sigma$ ) for the parameters after the adjustment is obtained as

$$\Sigma_X = N^{-1}.$$

If  $F$  is a  $w$ -vector of linear combinations of the parameters,

$$F = \bar{U}^T X,$$

where  $\bar{U}$  is a matrix of dimensions  $n \times w$ , one has

$$\Sigma_F = \bar{U}^T N^{-1} \bar{U},$$

which follows from the law of the variance-covariance propagation.

If  $N$  is nonsingular it is positive definite and it can be expressed as a product of a nonsingular matrix by its transpose, namely

$$N = T^T T .$$

In the "regular" Choleski algorithm (without the bandwidth considerations)  $T$  is in general an upper-triangular matrix with no other particular pattern and thus no special system of addressing. But this does not alter the present general considerations. In taking advantage of the triangular decomposition the following results are obtained at once:

$$X = T^{-1}R , \quad \Sigma_F = \overline{R^T R} ,$$

where

$$R = (T^T)^{-1}U , \quad \overline{R} = (T^T)^{-1}\overline{U} ,$$

and where the property  $N^{-1} = T^{-1}(T^T)^{-1}$  has been utilized.

In collecting the pertinent formulas, one first writes

$$T^T T = N , \quad T^T R = U , \quad T^T \overline{R} = \overline{U} ,$$

which can be represented by

$$T^T \left[ \begin{array}{c|c|c} T & R & \overline{R} \\ \hline n \times n & n \times 1 & n \times w \end{array} \right] = \left[ \begin{array}{c|c|c} N & U & \overline{U} \\ \hline n \times n & n \times 1 & n \times w \end{array} \right] , \quad (3.8a)$$

where the dimensions are also indicated. The remaining formulas of interest are

$$X = T^{-1} R, \quad (3.8b)$$

$n=1 \quad n=n \quad n=1$

$$\Sigma_F = \bar{R}^T \bar{R}.$$

$w=w \quad w=n \quad n=w$

The computation of the elements in  $T$ ,  $R$  and  $\bar{R}$  via (3.8a) is sometimes called "forward reduction" and the computation of  $X$  in (3.8b) may be called "back substitution".

The elements of  $T$  in (3.8a) are computed row by row, starting with the "ii" element and proceeding to the right until the "in" element is computed. The computation of the elements in  $R$  and  $\bar{R}$  follows the same algebraic pattern, to the extent that  $R$  and the columns in  $\bar{R}$  can be treated simply as additional columns to  $T$  (beyond the  $n$ -th column). If the computation proceeds as indicated, i.e., starting with the first element in the first row and following through with that row till completion, then starting with the "22" element, etc., the elements in  $T$ ,  $R$  and  $\bar{R}$  thus computed can replace the corresponding elements in  $N$ ,  $U$  and  $\bar{U}$  because the original elements in the latter three arrays will no longer be needed in the computations. This leads to savings of the core space where only  $N$  (upper triangular portion),  $U$  and  $\bar{U}$  need to be stored, becoming later  $T$  (upper-triangular),  $R$  and  $\bar{R}$ . During the step (3.8b), the elements of  $X$  may similarly replace the elements of  $R$  and thus the column which started originally as  $U$  will become  $X$  at the end of all the computations. The Choleski algorithm is then seen as performing the following transformations of elements in the same computer storage:

$$[N \ U \ \bar{U}] \rightarrow [T \ R \ \bar{R}] \rightarrow [T \ X \ \bar{R}] . \quad (3.9)$$

The algebraic operations carrying out (3.8a) in the "regular" Choleski algorithm (with "regular" addressing in T) are

$$t_{ii} = (n_{ii} - t_{1i}^2 - t_{2i}^2 - \dots - t_{i-1,i}^2)^{\frac{1}{2}} , \quad (3.10a)$$

$$t_{ij} = (n_{ij} - t_{1i}t_{1j} - t_{2i}t_{2j} - \dots - t_{i-1,i}t_{i-1,j})/t_{ii} , \quad (3.10b)$$

$$r_i = (u_i - t_{1i}r_1 - t_{2i}r_2 - \dots - t_{i-1,i}r_{i-1})/t_{ii} , \quad (3.10c)$$

$$\bar{r}_{ij'} = (\bar{u}_{ij'} - t_{1i}\bar{r}_{ij'} - t_{2i}\bar{r}_{2j'} - \dots - t_{i-1,i}\bar{r}_{i-1,j'})/t_{ii} . \quad (3.10d)$$

Here  $j$  starts with  $i+1$  and proceeds to  $n$  whereas  $j'$  proceeds from 1 to  $w$ , all for the given  $i$ ; subsequently  $i$  increases by one, and so on ( $i$  started with 1 and will end with  $n$ ). In the step (3.8b),  $i$  starts with  $n$ , then continues with  $n-1$ , etc., and ends with 1. Thus  $x_n$  is computed first,  $x_{n-1}$  follows in the process where the known  $x_n$  is also used, etc., hence the name "back substitution". With this provision (3.8b) translates into

$$x_i = (r_i - t_{in}x_n - t_{i,n-1}x_{n-1} - \dots - t_{i,i+1}x_{i+1})/t_{ii} , \quad (3.11)$$

which can start after the completion of the step (3.8a).

The next step is only intermediate and corresponds to (3.10a-d) and (3.11) in the case of a banded  $N$  matrix, but without any change in addressing. Advantage is merely taken of the zeros outside the band in that they are disregarded and not used in computations. A remark to be made with regard to the indices is that in (3.12a-d) below they can be



only positive (zero and negative indices are disregarded), that  $j$  in (3.12b) ends with  $i+b'$  or  $n$ , whichever is smaller, and that indices larger than  $n$  in (3.13) are disregarded.

$$t_{ii} = (n_{ii} - t_{i-b+1,i}^2 - t_{i-b+2,i}^2 - \dots - t_{i-1,i}^2)^{\frac{1}{2}}, \quad (3.12a)$$

$$t_{ij} = (n_{ij} - t_{j-b+1,i} t_{j-b+1,j} - t_{j-b+2,i} t_{j-b+2,j} - \dots - t_{i-1,i} t_{i-1,j}) / t_{ii}, \quad (3.12b)$$

$$r_i = (u_i - t_{i-b+1,i} r_{i-b+1} - t_{i-b+2,i} r_{i-b+2} - \dots - t_{i-1,i} r_{i-1}) / t_{ii}, \quad (3.12c)$$

$$\bar{r}_{ij} = (u_{ij} - t_{i-b+1,i} \bar{r}_{i-b+1,j} - t_{i-b+2,i} \bar{r}_{i-b+2,j} - \dots - t_{i-1,i} \bar{r}_{i-1,j}) / t_{ii}; \quad (3.12d)$$

$$x_i = (r_i - t_{i,i+1} x_{i+1} - t_{i,i+2} x_{i+2} - \dots - t_{i,i+b-1} x_{i+b-1}) / t_{ii}. \quad (3.13)$$

Finally, advantage is taken of the banded structure of  $N$  by replacing it with  $\tilde{T}$  described previously. This entails the change in addressing presented as (3.7a,b). The matrix  $T$  then also changes its shape and addressing; for this reason it should perhaps be called by a different name, but here the symbol " $T$ " is retained with the knowledge that it is now a rectangular matrix of dimensions  $b \times n$ . This having been said, the elements in the (new)  $T$  matrix, in  $R$  and  $\bar{R}$ , and finally in  $X$  are presented below where, in addition to (3.6), also the following notation is used:

$$b'' = b' - (j - i). \quad (3.14)$$

The formulas are written in their final form convenient for programming. The principal index  $i$  runs again from 1 to  $n$ , the index  $j$  within each  $i$  ends again with  $\inf(i-b', n)$ , etc.

$$t_{bi} = (\tilde{t}_{bi} - \sum_{\ell=1}^{b'} t_{\ell i}^2)^{1/2}, \quad (3.15a)$$

$$t_{b-(j-i),j} = (\tilde{t}_{b-(j-i),j} - \sum_{\ell=1}^{b''} t_{j-i+\ell,i} t_{\ell j}) / t_{bi}, \quad (3.15b)$$

$$i < b: \quad r_i = (u_i - \sum_{\ell=1}^{i-1} t_{b-i+\ell,i} r_{\ell}) / t_{bi}, \quad (3.15c)$$

$$i \geq b: \quad r_i = (u_i - \sum_{\ell=1}^{b'} t_{\ell i} r_{i-b+\ell}) / t_{bi}, \quad (3.15c')$$

$$i < b: \quad \bar{r}_{ij} = (\bar{u}_{ij} - \sum_{\ell=1}^{i-1} t_{b-i+\ell,i} \bar{r}_{\ell j}) / t_{bi}, \quad (3.15d)$$

$$i \geq b: \quad \bar{r}_{ij} = (\bar{u}_{ij} - \sum_{\ell=1}^{b'} t_{\ell i} \bar{r}_{i-b+\ell,j}) / t_{bi}; \quad (3.15d')$$

$$x_i = (r_i - \sum_{\ell=1}^{\inf(b', n-i)} t_{b-\ell, i+\ell} x_{i+\ell}) / t_{bi}. \quad (3.16)$$

Instead of the full variance-covariance matrix of  $F$ , only the chosen sigmas and the correlation coefficients will be computed. The input parameters will be the pairs  $j'_1$  and  $j'_2$  which will serve to choose the appropriate columns of  $\bar{R}$  and compute the desired values as follows:

$$\sigma_{j'_1} = \left( \sum_{\ell=1}^n \bar{r}_{\ell j'_1}^2 \right)^{1/2}, \quad (3.17a)$$

$$\sigma_{j'_2} = \left( \sum_{\ell=1}^n \bar{r}_{\ell j'_2}^2 \right)^{1/2}, \quad (3.17b)$$

$$\rho_{j'_1 j'_2} = \left( \sum_{\ell=1}^n \bar{r}_{\ell j'_1} \bar{r}_{\ell j'_2} \right) / (\sigma_{j'_1} \sigma_{j'_2}). \quad (3.17c)$$

Some economies can be realized if one takes into account that several elements in the columns of  $\bar{U}$  may be zeros; however, only those zero elements which precede the first nonzero element are beneficial. Similar considerations could apply also with regard to  $U$  but this is merely a theoretical case since as a rule  $U$  is a full vector. Suppose that in a column  $j'$  of  $\bar{U}$  the first nonzero element is at the address  $i=J'$ . Then the first nonzero element in the  $j'$ -th column of  $\bar{R}$  appears also at the address  $i=J'$  so that the computations of the preceding elements as in (3.15d), (3.15d') can be skipped and these elements can be set directly to zero. Furthermore, the multiplications on the right-hand sides of (3.15d), (3.15d') with these zero elements can likewise be skipped, in other words,  $\ell=1$  in the summations can be replaced with the appropriate  $J'$ . In the same vein,  $\ell=1$  in (3.17a,b) can be replaced by the corresponding  $J'_1$  and  $J'_2$ , respectively, and  $\ell=1$  in (3.17c) can be replaced by  $\sup(J'_1, J'_2)$ .

Finally, one notices that the symbolism (3.9) would, in the modified Choleski algorithm, read as

$$\begin{matrix} \tilde{T} & U & \bar{U} & \rightarrow & T & R & \bar{R} & \rightarrow & T & X & \bar{R} \\ b \times n & n \times 1 & n \times w & & b \times n & n \times 1 & n \times w & & b \times n & n \times 1 & n \times w \end{matrix} \quad (3.18)$$

The brackets have been left out because the complete expression is not one matrix.

The approach utilizing the P.M. parameters is based on the residuals from a previous global adjustment in terms of spherical-harmonic potential coefficients. The P.M. approach considers the residuals in the exact locations on the globe where the actual altimeter measurements took place.

There are other interpolation and approximation techniques where the observations are "translocated" to some strategically advantageous positions, such as to grid locations (equilateral, geographical, etc.). Such techniques may be very crude (the location is considered shifted but the value is taken without any correction) or quite elaborate (e.g., as in the "best linear prediction" method). Since the values at shifted locations are estimated and not measured, any such technique entails approximations which are avoided in the P.M. adjustment. As a trade-off, some of the above techniques are very efficient computationally. The present approach with the modified Choleski algorithm seeks to improve the computational efficiency while relaxing the rigor of the solution as little as possible.

#### 4. MODEL FOR DEFLECTION RATES IN TERMS OF SPHERICAL HARMONICS AND POINT MASSES

The need to develop mathematical foundations for new observational modes is dictated by the surge in various new or improved operational systems. For example, broad advances have been made in the area of inertial instrumentation which has been used with growing success in inertial navigation. In using this instrumentation, the observational process can be designed to yield differential changes in the deflections of the vertical along a given route. Thus the quantities to be modeled by a given set of parameters, such as the spherical-harmonic (S.H.) potential coefficients or the point mass (P.M.) magnitudes, can be viewed as the deflection rates at chosen (observational) points. Such points would usually be distributed along profiles whose azimuth is denoted by  $\alpha$ . At each point the measured quantities to be modeled are denoted as  $\dot{\xi}$  and  $\dot{\eta}$ , associated with a specific  $\alpha$ . This type of data involves second derivatives of the disturbing potential (T) with respect to length elements (ds), which could be particularly useful for the resolution of short-wavelength features in a local gravity field. The development contained herein is based on [Hotine, 1969] abbreviated as [H] and on [Blaha, 1980] abbreviated as [B]. It could be considered, in fact, to be an extension of Chapter 4 in [B] insofar as the S.H. and P.M. (single layer) parameters are concerned, and it could follow Section 4.6 in this reference.

#### 4.1 Mathematical Background

Similar to the material contained in paragraph 19 on page 7 of [H], the derivative of a function  $F$  with respect to the length element along a desired direction reads

$$\partial F / \partial s = (\partial F / \partial x^r)(\partial x^r / \partial s) \equiv F_r p^r,$$

which is an invariant (independent of the coordinate system represented by  $x^r$ ), where

$F_r$  = gradient of  $F$  ,

$p^r$  = unit vector in the desired direction,  
whose length element is  $ds$ .

In the present context,  $p^r$  lies in a level surface and its azimuth is  $\alpha$ .

Similar to equation 12.006 of [H] we write

$$p^r = \ell_{(1)}^r \sin \alpha + \ell_{(2)}^r \cos \alpha,$$

where (1) refers to an easterly direction along which the differential distance is denoted  $ds_E$  and (2) refers to a northerly direction associated with  $ds_N$ . In the spherical coordinate system  $\{\lambda, \bar{\phi}, r\}$ , the first two coordinates are the geocentric longitude and latitude, respectively, and the third is the geocentric radial distance. In agreement with (3.48) of [B] we have

$$\ell_{(1)}^r = \{1/(r \cos \bar{\phi}), 0, 0\}, \quad \ell_{(2)}^r = \{0, 1/r, 0\},$$

$$p^r = \{(1/r \cos \bar{\phi}) \sin \alpha, (1/r) \cos \alpha, 0\}, \quad (4.1)$$

where the index "r" should not be confused with the radial distance denoted by the same letter. Here and in the sequel,  $(1/r \cos \bar{\phi})$ , etc., are written to represent  $[1/(r \cos \bar{\phi})]$ , etc., since the latter notation would sometimes contribute to a profusion of parentheses and brackets; there is no need for the former notation to be confused with  $(1/r) \cos \bar{\phi}$ . As is customary with tensor notations, the summation convention applies.

If  $\partial F / \partial s$  represents a deflection of the vertical (the sign change follows from the convention explained on page 79 of [B]),  $F$  becomes the geoid undulation  $N$  and we write for the deflections in the north and east directions, respectively:

$$\xi \equiv -\partial N / \partial s_N = -N_r \ell_{(2)}^r = -(1/r) \partial N / \partial \bar{\phi} , \quad (4.2)$$

$$\eta \equiv -\partial N / \partial s_E = -N_r \ell_{(1)}^r = -(1/r \cos \bar{\phi}) \partial N / \partial \lambda . \quad (4.3)$$

The rates of these quantities along the general azimuth  $\alpha$ , along  $\alpha=0$  and along  $\alpha=90^\circ$  are expressed as

$$\dot{\xi} \equiv \partial \xi / \partial s \equiv -\partial^2 N / \partial s_N \partial s = \xi_r p^r , \quad (4.4)$$

$$\dot{\eta} \equiv \partial \eta / \partial s \equiv -\partial^2 N / \partial s_E \partial s = \eta_r p^r ; \quad (4.5)$$

$$\dot{\xi}_N \equiv \partial \xi / \partial s_N \equiv -\partial^2 N / \partial s_N^2 = \xi_r \ell_{(2)}^r ,$$

$$\dot{\eta}_N \equiv \partial \eta / \partial s_N \equiv -\partial^2 N / \partial s_E \partial s_N = \eta_r \ell_{(2)}^r ;$$

$$\dot{\xi}_E \equiv \partial \xi / \partial s_E \equiv -\partial^2 N / \partial s_N \partial s_E = \xi_r \ell_{(1)}^r ,$$

$$\dot{\eta}_E \equiv \partial \eta / \partial s_E \equiv -\partial^2 N / \partial s_E^2 = \eta_r \ell_{(1)}^r .$$

The above relations do not mean that the same formulas will be recovered for  $\dot{\xi}_E$  and  $\dot{\eta}_N$ . Instead, another relationship will be derived for checking purposes. First suppose that scalar functions of position  $F$  and  $H$  are such that

$$H = \partial F / \partial s \equiv F_r p^r .$$

Next identify another direction and its unit vector, etc., by primes, namely

$$H' = \partial F / \partial s' \equiv F_r p'^r .$$

Two kinds of derivatives are now formed:

$$\partial H / \partial s' = \partial^2 F / \partial s \partial s' \equiv (F_r p^r)_s p'^s ,$$

$$\partial H' / \partial s = \partial^2 F / \partial s' \partial s \equiv (F_r p'^r)_s p^s .$$

Using the rules for covariant differentiation according to Chapter 3 of [H], we have

$$(F_r p^r)_s = F_{rs} p^r + F_r p^r_s ,$$

$$p^r_s = \partial p^r / \partial x^s + \Gamma^r_{sk} p^k ;$$

the symbols  $F_{rs}$ ,  $\Gamma^r_{sk}$ , symmetric in the lower indices, eventually cancel out and need not be elaborated upon. Straightforward algebra yields

$$\partial^2 F / \partial s' \partial s - \partial^2 F / \partial s \partial s' = F_r [(\partial p'^r / \partial x^s) p^s - (\partial p^r / \partial x^s) p'^s] . \quad (4.6)$$



We now associate  $F$  with  $N$  and, anticipating the spherical approximation, write

$$N = (1/G)T, \quad (4.7)$$

where  $G$  is the average value of gravity at the earth's surface (approximately 980 gals). Equation (4.7) follows from the Bruns formula presented on page 85 of [Heiskanen and Moritz, 1967]. If  $ds$  and  $ds'$  are identified with  $ds_N$  and  $ds_E$ , respectively, and other quantities are identified accordingly, it is readily deduced that

$$\partial^2 N / \partial s_E \partial s_N - \partial^2 N / \partial s_N \partial s_E \equiv \dot{\xi}_E - \dot{\eta}_N = (1/Gr^2 \cos \bar{\phi}) \operatorname{tg} \bar{\phi} \partial T / \partial \lambda. \quad (4.8)$$

In analogy to  $G$  in (4.7),  $r$  in the final formula can be substituted for by  $R$ , the earth's mean radius (approximately 6371 km), for the deflection rates as modeled customarily for the earth's surface.

In considering (4.1) and (4.7), the formulas (4.2) - (4.5) yield

$$\dot{\xi} = -(1/Gr^2) [(1/\cos \bar{\phi}) (\partial^2 T / \partial \lambda \partial \bar{\phi}) \sin \alpha + (\partial^2 T / \partial \bar{\phi}^2) \cos \alpha], \quad (4.9)$$

$$\dot{\eta} = -(1/Gr^2 \cos \bar{\phi}) [(1/\cos \bar{\phi}) (\partial^2 T / \partial \lambda^2) \sin \alpha + (\operatorname{tg} \bar{\phi} \partial T / \partial \lambda + \partial^2 T / \partial \lambda \partial \bar{\phi}) \cos \alpha]. \quad (4.10)$$

However, if the computation of  $\partial^2 T / \partial \bar{\phi}^2$  is sought to be avoided as in the S.H. model, one can take advantage of the Laplace condition for harmonic functions, in particular,

$$\Delta T = 0.$$

The alternate formula for  $\dot{\xi}$  then reads

(4.9')

$$\dot{\xi} = -(1/G)\{(1/r \cos\bar{\phi})(\partial^2 T/\partial\lambda\partial\bar{\phi})\sin\alpha + [-(1/r^2 \cos^2\bar{\phi})\partial^2 T/\partial\lambda^2 - \partial^2 T/\partial r^2 + (tg\bar{\phi}/r^2)\partial T/\partial\bar{\phi} - (2/r)\partial T/\partial r]\cos\alpha\},$$

where the expression inside the brackets replaces  $\partial^2 T/\partial\bar{\phi}^2$  in (4.9). Upon setting  $\alpha=90^\circ$  in (4.9) or (4.9'), and  $\alpha=0$  in (4.10), the verification equation (4.8) follows. If the formulas for the deflection rates in spherical approximation should be used at aircraft or satellite altitudes,  $r$  and  $G$  values above would be substituted for by their counterparts for the geop in question.

## 4.2 Spherical-Harmonic Approach

In spherical approximation, the selected formulas in (3.77) of [B] for  $r=R$  can be rewritten in terms of a set of S.H. potential coefficients truncated at  $n=N$  as

$$\left. \begin{aligned}
 \partial T / \partial \lambda &= RG \sum_{n=2}^N \Delta S'(n) , \\
 \partial T / \partial \bar{\phi} &= RG \sum_{n=2}^N \Delta \bar{S}(n) , \\
 \partial T / \partial r &= -G \sum_{n=2}^N (n+1) \Delta S(n) , \\
 \partial^2 T / \partial \lambda^2 &= RG \sum_{n=2}^N \Delta S''(n) , \\
 \partial^2 T / \partial \lambda \partial \bar{\phi} &= RG \sum_{n=2}^N \Delta \bar{S}'(n) , \\
 \partial^2 T / \partial r^2 &= (G/R) \sum_{n=2}^N (n+1)(n+2) \Delta S(n) ,
 \end{aligned} \right\} (4.11)$$

where the notations, according to (3.76) and (3.78a-d) of [B], are

$$\left. \begin{aligned}
 \Delta S(n) &= \sum_{m=0}^n (\Delta C_{nm} \cos m\lambda + \Delta S_{nm} \sin m\lambda) P_{nm}(\sin \bar{\phi}) , \\
 \Delta S'(n) \equiv \partial \Delta S / \partial \lambda &= \sum_{m=0}^n m (-\Delta C_{nm} \sin m\lambda + \Delta S_{nm} \cos m\lambda) P_{nm}(\sin \bar{\phi}) ,
 \end{aligned} \right\}$$

$$\begin{aligned}
\Delta S''(n) &\equiv \partial^2 \Delta S / \partial \lambda^2 = - \sum_{m=0}^n m^2 (\Delta C_{nm} \cos m\lambda + \Delta S_{nm} \sin m\lambda) P_{nm}(\sin \bar{\phi}) , \\
\Delta \bar{S}(n) &\equiv \partial \Delta S / \partial \bar{\phi} = \sum_{m=0}^n (\Delta C_{nm} \cos m\lambda + \Delta S_{nm} \sin m\lambda) dP_{nm}(\sin \bar{\phi}) / d\bar{\phi} , \\
\Delta \bar{S}'(n) &\equiv \partial^2 \Delta S / \partial \lambda \partial \bar{\phi} = \sum_{m=0}^n m (-\Delta C_{nm} \sin m\lambda + \Delta S_{nm} \cos m\lambda) dP_{nm}(\sin \bar{\phi}) / d\bar{\phi} .
\end{aligned}
\quad \left. \vphantom{\sum_{m=0}^n} \right\} (4.12)$$

With  $C_{no}^*$  representing the reference field, the notations are

$$\Delta C_{no} = C_{no} - C_{no}^*$$

for  $n=2, 4$  and perhaps  $6$ , the remaining  $\Delta C_{nm}$  and all of the  $\Delta S_{nm}$  being the coefficients  $C_{nm}$  and  $S_{nm}$  themselves.

Upon utilizing the notations (4.11), (4.12), the formulas (4.9') and (4.10) lead to

$$\begin{aligned}
\dot{\xi} = & -(1/R) \{ (1/\cos \bar{\phi}) \sum_{n=2}^N \Delta \bar{S}'(n) \sin \alpha - [(1/\cos^2 \bar{\phi}) \sum_{n=2}^N \Delta S''(n) \\
& + \sum_{n=2}^N n(n+1) \Delta S(n) - \operatorname{tg} \bar{\phi} \sum_{n=2}^N \Delta \bar{S}(n)] \cos \alpha \} , \quad (4.13)
\end{aligned}$$

$$\begin{aligned}
\dot{\eta} = & -(1/R \cos \bar{\phi}) \{ (1/\cos \bar{\phi}) \sum_{n=2}^N \Delta S''(n) \sin \alpha + [\operatorname{tg} \bar{\phi} \sum_{n=2}^N \Delta S'(n) \\
& + \sum_{n=2}^N \Delta \bar{S}'(n)] \cos \alpha \} . \quad (4.14)
\end{aligned}$$

If  $\alpha=90^\circ$  and  $\alpha=0$  are used in (4.13) and (4.14), respectively, the verification equation (4.8) follows upon utilizing the notation from the first equation of (4.11).

In following the same sequence of derivations as in [B], the partial derivatives of the above quantities with respect to the S.H. coefficients are expressed as

$$\partial \dot{\xi} / \partial C_{no} = (1/R) [n(n+1) P_n(\sin \bar{\phi}) - \operatorname{tg} \bar{\phi} dP_n(\sin \bar{\phi}) / d\bar{\phi}] \cos \alpha ,$$

$$\partial \dot{\xi} / \partial C_{nm} = (1/R) (A \sin m\lambda - B \cos m\lambda) ,$$

$$\partial \dot{\xi} / \partial S_{nm} = -(1/R) (A \cos m\lambda + B \sin m\lambda) ;$$

$$\partial \dot{\eta} / \partial C_{no} = 0 ,$$

$$\partial \dot{\eta} / \partial C_{nm} = (m/R \cos \bar{\phi}) (C \cos m\lambda + D \sin m\lambda) ,$$

$$\partial \dot{\eta} / \partial S_{nm} = (m/R \cos \bar{\phi}) (C \sin m\lambda - D \cos m\lambda) ;$$

the new notations in these expressions are

$$A = (m/\cos \bar{\phi}) [dP_{nm}(\sin \bar{\phi}) / d\bar{\phi}] \sin \alpha ,$$

$$B = \{ [(1/\cos^2 \bar{\phi}) m^2 - n(n+1)] P_{nm}(\sin \bar{\phi}) + \operatorname{tg} \bar{\phi} dP_{nm}(\sin \bar{\phi}) / d\bar{\phi} \} \cos \alpha ;$$

$$C = (m/\cos \bar{\phi}) P_{nm}(\sin \bar{\phi}) \sin \alpha ,$$

$$D = [\operatorname{tg} \bar{\phi} P_{nm}(\sin \bar{\phi}) + dP_{nm}(\sin \bar{\phi}) / d\bar{\phi}] \cos \alpha .$$

### 4.3 Approach Using a Single Layer of Point Masses

The notations in this analysis will be the same as those used in [B], pages 67 and 68 for the point masses located at the depth  $d$  below the sphere of radius  $R$ :

$$T_i = \sum_j (1/\ell_{ij})(kM)_j, \quad (4.15)$$

where

$$\begin{aligned} \ell_{ij} &= (R^2 - R_1^2 - 2F_{ij})^{\frac{1}{2}}, \\ &= \text{the distance between the } i\text{-th (observation) point and the } j\text{-th point mass,} \\ R_1 &= R - d, \\ d &= 0.8 s, \\ s &= \text{the horizontal separation between point masses considered in an equilateral grid in the adjustment model,} \\ F_{ij} &= RR_1 \cos \psi_{ij}, \\ \cos \psi_{ij} &= \sin \phi_i \sin \phi_j + \cos \phi_i \cos \phi_j \cos \Delta \lambda_{ij}, \\ \Delta \lambda_{ij} &= \lambda_i - \lambda_j, \\ (kM)_j &= \text{the } j\text{-th scaled P.M. magnitude,} \\ \phi_k, \lambda_k &= \text{the geocentric coordinates of a point } k \text{ (either } i \text{ or } j\text{).} \end{aligned} \quad (4.15')$$

In the case the observation points should not be at the earth's surface but at aircraft or satellite altitudes (then  $R$  is larger than 6371 km),  $d$  may have to be increased beyond the value indicated above if the locations of the point masses are still desired to be underneath the actual earth's surface.

The deflection rates at the observation point  $i$  can be transcribed, in spherical approximation, from (4.9) and (4.10) as follows:

$$\dot{\xi}_i = -(1/GR^2) [(1/\cos\phi_i)(\partial^2 T_i / \partial \lambda_i \partial \phi_i) \sin\alpha + (\partial^2 T_i / \partial \phi_i^2) \cos\alpha] , \quad (4.16)$$

$$\dot{\eta}_i = -(1/GR^2 \cos\phi_i) [(1/\cos\phi_i)(\partial^2 T_i / \partial \lambda_i^2) \sin\alpha + (\text{tg}\phi_i \partial T_i / \partial \lambda_i + \partial^2 T_i / \partial \lambda_i \partial \phi_i) \cos\alpha] . \quad (4.17)$$

The required partial derivatives of  $T_i$  can be found from (4.15), and they are listed as (4.7a-i) in [B]. Using these derivatives, after a few algebraic manipulations we find

$$\dot{\xi}_i = (R_1/GR) \sum_j (1/\ell_{ij}^3) [(1/\cos\phi_i)(p_{ij}t_{ij} - \text{tg}\phi_i)q_{ij} \sin\alpha - (p_{ij}t_{ij}^2 - \cos\psi_{ij})\cos\alpha](\text{km})_j , \quad (4.18)$$

$$\dot{\eta}_i = -(R_1/GR \cos\phi_i) \sum_j (1/\ell_{ij}^3) [(1/\cos\phi_i)(p_{ij}q_{ij}^2 - \cos\phi_i \cos\phi_j \cos\Delta\lambda_{ij}) \sin\alpha - p_{ij}q_{ij}t_{ij} \cos\alpha](\text{km})_j , \quad (4.19)$$

where

$$p_{ij} = 3RR_1/\ell_{ij}^2 ,$$

$$t_{ij} = \cos\phi_i \sin\phi_j - \sin\phi_i \cos\phi_j \cos\Delta\lambda_{ij} ,$$

$$q_{ij} = \cos\phi_i \cos\phi_j \sin\Delta\lambda_{ij} .$$

Next we consider (4.18) and (4.19) for one point mass  $j$  and vary the position of the observation point  $i$  by distances  $ns$ , where  $n$  is the number of intervals  $s$  along a general direction. As in [B], this strategy makes it possible to see at how many intervals away from the observation point the P.M. parameters still significantly affect the modeled value (and vice versa), and should be included in the pertinent observation equation or prediction formula. The inclusion of all the P.M. parameters in a large-area adjustment would entail prohibitive computer core and run-time requirements. The consideration of only one point mass removes the summation signs in (4.18) and (4.19). As in [B] in comparable situations, the latitude of  $j$  is chosen zero,  $\phi_j=0$ , which here simplifies also the formulas for  $t_{ij}$ ,  $q_{ij}$  and  $\cos\psi_{ij}$ . Since we are dealing with small changes, first-order approximations are further introduced, such as

$$\cos\Delta\lambda_{ij} = 1 , \quad \sin\Delta\lambda_{ij} = \Delta\lambda_{ij} ,$$

$$\cos\phi_i = 1 , \quad \sin\phi_i = \Delta\phi_{ij} ,$$

etc., where

$$\phi_i = \phi_i - \phi_j \equiv \Delta\phi_{ij} .$$



In carrying out the straightforward algebra (in this process one also realizes that  $p_{ij}$  is about two orders of magnitude greater than  $\Delta\phi_{ij}$ ), it follows from (4.18) and (4.19) that

$$\dot{\xi}_i = -(R_1/GR)(1/\ell_{ij}^3)[p_{ij}\Delta\phi_{ij}\Delta\lambda_{ij}\sin\alpha + (p_{ij}\Delta\phi_{ij}^2 - 1)\cos\alpha](\text{km})_j, \quad (4.20)$$

$$\dot{\eta}_i = -(R_1/GR)(1/\ell_{ij}^3)[(p_{ij}\Delta\lambda_{ij}^2 - 1)\sin\alpha + p_{ij}\Delta\phi_{ij}\Delta\lambda_{ij}\cos\alpha](\text{km})_j. \quad (4.20')$$

Clearly, whatever values are obtained for  $\dot{\xi}_i$  with a given azimuth  $\alpha=\alpha'$ , are also the values obtained for  $\dot{\eta}_i$  with  $\alpha=90^\circ-\alpha'$ , and with  $\Delta\phi_{ij}$  and  $\Delta\lambda_{ij}$  interchanged. Therefore, it is sufficient to examine only one of these equations, for example (4.20), with regard to cut-off considerations in the "worst situation". Such a situation depicts the greatest influence of the P.M. at  $j$  upon the modeled value at  $i$  at various distances  $j-i$ , both with respect to  $\alpha$  and  $\beta$ , where  $\beta$  is the azimuth measured from  $j$  to  $i$ .

In angular measure  $s$  is denoted as  $\Delta\omega$  and the angular distances between  $j$  and  $i$  proceed in  $n$ -multiples of  $\Delta\omega$ . We then have

$$\psi_{ij} = n \Delta\omega, \quad \Delta\phi_{ij} = n \Delta\omega \cos\beta, \quad \Delta\lambda_{ij} = n \Delta\omega \sin\beta. \quad (4.21)$$

In view of (4.20), the following approximate relations are developed:

$$\left. \begin{aligned} \ell_{ij}^2 &\approx R^2 \Delta\omega^2 (n^2 + 0.64), \\ p_{ij} &\approx 3/[\Delta\omega^2 (n^2 + 0.64)] \end{aligned} \right\} \quad (4.22)$$

where  $d=0.8s$  from (4.15') in angular measure has been taken into account.

Equation (4.20) thus becomes

$$\dot{\xi}_i = -C[1/(n^2 + 0.64)^{5/2}][3n^2 \sin\beta \cos\beta \sin\alpha + (3n^2 \cos^2\beta - n^2 - 0.64)\cos\alpha] , \quad (4.23)$$

$$C = R_1(kM)_j / (GR^4 \Delta\omega^3) . \quad (4.23')$$

In order to find the worst situation, the function  $f(\alpha, \beta)$  forming the second brackets in (4.23) is examined for local extremes, where

$$f(\alpha, \beta) = a \sin\beta \cos\beta \sin\alpha + (b \cos^2\beta - c)\cos\alpha , \quad (4.24)$$

$$a = 3n^2 , \quad b = 3n^2 , \quad c = n^2 + 0.64 . \quad (4.24')$$

One first forms  $\partial f/\partial\alpha = 0$  and  $\partial f/\partial\beta = 0$  and seeks the solution for  $\beta$ , for example, after having eliminated  $\alpha$ . The result is represented by

$$\cos^2\beta = (2bc - a^2)/[2(b^2 - a^2)] .$$

Without any further analysis one notices that such a local extreme does not exist due to  $a=b$  in (4.24'). One can then proceed by examining different azimuths  $\alpha$ , held fixed, and searching for an extreme with respect to  $\beta$ . In using this approach, the azimuths  $\alpha=0, 45^\circ$  and  $90^\circ$  are adopted.

Azimuth  $\alpha=0$ . Here the second brackets in (4.23) contain only the second term (with  $\cos\alpha$  replaced by 1). This is then called  $f(\beta)$  whose local extremes are sought. Simple algebraic manipulations reveal that an extreme occurs at  $\beta=0$  and that it represents a maximum; the second derivative of  $f(\beta)$  with respect to  $\beta$  evaluated with  $\beta=0$  is negative. However, we are

interested in a maximum in absolute value, which is seen to coincide with the maximum just found when  $f(\beta)$  reaches at least  $n^2 + 0.64$ . With  $\beta=0$  this happens whenever  $n > 1.13$ . Since we are especially concerned with the distances  $j-i$  in the vicinity of  $1.5s$ , the results implied by the above procedure are satisfactory. Thus, upon disregarding the signs the formula and the values below represent the absolute maximum for the intervals of interest:

$$\alpha=0, \quad \beta=0; \quad \dot{\xi}_i = -C[(2n^2 - 0.64)/(n^2 + 0.64)^{5/2}] ; \quad (4.25)$$

$n = 0$	.....	100%	$n = 1$	.....	-20.3%	}	(4.25')
$n = 0.5$	.....	9.6%	$n = 1.5$	.....	-13.9%		
			$n = 2$	.....	- 8.2%		

Note: The formula (4.25), examined for  $n$ , reveals a primary maximum at  $n=0$  associated with "100%", and a secondary maximum at  $n=1$  (more precisely at  $n=0.98$ ).

Azimuth  $\alpha=45^\circ$ . In this case both  $\sin\alpha$  and  $\cos\alpha$  in (4.23) are replaced by 0.7071 taken out of the brackets. A maximum for the new  $f(\beta)$  occurs at  $\beta=22.5^\circ$  and it corresponds to the absolute maximum already for  $n > 0.89$ , which is entirely satisfactory. Similar to (4.25), (4.25'), this configuration is represented by

$$\alpha=45^\circ, \quad \beta=22.5^\circ; \quad \dot{\xi}_i = -C(0.7071)[(2.62n^2 - 0.64)/(n^2 + 0.64)^{5/2}]; \quad (4.26)$$

$n = 0$	.....	100%	$n = 1$	.....	-29.5%	} (4.26')
$n = 0.5$	.....	-1.0%	$n = 1.5$	.....	-19.0%	
$n = 0.91$	.....	-30.1%	$n = 2$	.....	-10.9%	

Note: In addition to the primary maximum at  $n=0$ , the formula (4.26) has a secondary maximum at  $n=0.91$ .

Azimuth  $\alpha=90^\circ$ . Now only the first term inside the second brackets in (4.23) remains, for which the (absolute) maximum occurs at  $\beta=45^\circ$ . This situation is depicted as follows:

$$\alpha=90^\circ, \quad \beta=45^\circ; \quad \dot{\xi}_i = -C[1.5n^2/(n^2 + 0.64)^{5/2}] ; \quad (4.27)$$

$n = 0$	.....	0	$n = 1$	.....	-79.8%	} (4.27')
$n = 0.5$	.....	- 92%	$n = 1.5$	.....	-43.7%	
$n = 0.65$	.....	-100%	$n = 2$	.....	-23.7%	
			$n = 2.5$	.....	-13.8%	

Note: The formula (4.27) reveals only the primary maximum at  $n=0.65$ .

In closing this part of the analysis, we comment that due to the symmetry in the deflection-rate formulas in conjunction with the point mass  $j$  located in the vicinity of the observation point  $i$ , it is sufficient to consider the azimuths  $\alpha$  and  $\beta$  in the first quadrant. In examining three representative azimuths  $\alpha$  ( $0, 45^\circ, 90^\circ$ ) in conjunction with  $\dot{\xi}_i$ , it is noticed that  $\alpha=90^\circ$  depicts, by far, the "worst" situation. At  $\alpha=0$  the influence (at  $i$ ) of the point mass (at  $j$ ) is felt the least; the situation for  $\alpha=45^\circ$  is only slightly "worse". But even for  $\alpha=90^\circ$  the cut-off distance of  $1.5s$  corresponding to 43.7% is acceptable. Although it may be

deemed marginal, it is still somewhat more satisfactory than the same distance in the case of geoid undulations (under similar circumstances, 1.5s for geoid undulations is associated with 47.6%). In summary, the "worst situation" corresponds to  $\dot{\xi}_i$  for  $\alpha=90^\circ$  or to  $\dot{\eta}_i$  for  $\alpha=0$ , with  $\beta=45^\circ$  in both cases (interchanging  $\Delta\phi_{ij}$  and  $\Delta\lambda_{ij}$  does not matter here). In other words, most affected by a given point mass are the rates of change in  $\xi$  along the E-W direction and in  $\eta$  along the N-S direction, as modeled at observation points located along the NE (and NW, etc.) direction from that point mass.

## 5. OBSERVATION MODES IN TERMS OF A DOUBLE LAYER OF POINT MASSES

An analogy between the point-mass representation of the potential and the density layer representation has been exploited in the past. If also the double density layer concept is applied to the point-mass model, it leads to the notion of a dipole. As in the double layer situation, two point masses (P.M.) of the same magnitude but opposite signs can be imagined located along the same normal to the reference surface. The depth, underneath the earth's surface, of the upper P.M. is denoted by  $d$  as in the single P.M. approach. The depth of the lower, newly added P.M. is denoted by

$$d' = d + v ,$$

where  $v$  is the vertical separation between the twin point masses. And, similar to the approach with the single P.M., the horizontal separation between the neighboring twin P.M. is denoted by  $s$ .

In analogy to the concept of double layer, the minus mass (or minus density) has no direct physical meaning in itself but is a useful mathematical device. Although the number of P.M. themselves doubles with respect to the single P.M. approach, the number of parameters remains the same due to the condition that the P.M. along the surface normal differ only in sign, not in magnitude. If  $v$  and thus also the depth of the lower P.M. grows indefinitely, the characteristics of the single P.M. layer are recovered. On the other hand, the decrease in  $v$  leads to different characteristics which may be desirable in some respects. For example,

if  $v$  becomes sufficiently small compared to  $s$ , such as  $v = 0.112s$  used herein (corresponding to  $v = 50$  km for  $s = 445$  km), the relative effect of a twin P.M. on the modeled value decreases much more rapidly with distance than that of a single P.M. With even smaller  $v$  this feature is further accentuated.

The above discussion implies that a given cut-off distance in the double layer approach introduces fewer approximations in the adjustment model than does the same distance in the single layer approach (under the implied assumption of constant  $d$ ). The cut-off distance is defined in [Blaha, 1980] as the distance from an observation point beyond which no P.M. parameters are considered in the formation of the pertinent observation equation. If one tolerates about the same level of approximation in both approaches, one can decrease the cut-off distance in the twin P.M. model and thereby alleviate the computer run-time requirements. In the present analysis the cut-off distance corresponds to  $1.5s$ ; the resulting approximations in the double P.M. approach will be seen to be mostly inconsequential.

The present development is based in several respects on [Blaha, 1980], abbreviated here as [B]. The first section below is concerned with developing the twin P.M. model for five observational (and prediction) modes as presented in [B]. The five kinds of modeled quantities are: geoid undulations, gravity anomalies, deflections of the vertical (north and east), horizontal gradients of gravity disturbance (north and east), and vertical gradients of gravity disturbance. The subsequent section deals with the twin P.M. concept applied to the new observational mode, the deflection rates. Since both sections are intended to be essentially independent, minor overlaps occur in a few instances.

## 5.1 Adaptation of Five Observational Modes to Twin Point Masses

The geoid undulation at the (observation) point  $i$  due to single point masses is, according to [B], equation (4.17):

$$N_i = (1/G) \sum_j (1/\ell_{ij})(kM)_j, \quad (5.1)$$

where

$\ell_{ij}$  = distance between the  $i$ -th (observation) point and the  $j$ -th point mass,

$(kM)_j$  =  $j$ -th scaled point-mass magnitude,

$$\ell_{ij} = (R^2 + R_1^2 - 2F_{ij})^{1/2}, \quad (5.2a)$$

$$R_1 = R - d, \quad (5.2b)$$

$$F_{ij} = R R_1 \cos\psi_{ij}, \quad (5.2c)$$

$$\cos\psi_{ij} = \sin\phi_i \sin\phi_j + \cos\phi_i \cos\phi_j \cos(\lambda_i - \lambda_j), \quad (5.2d)$$

where  $R$  represents the earth's mean radius (6.371 km),  $G$  is the average value of gravity on the earth's surface (980 gals), and where  $\psi_{ij}$  is the spherical distance between the points  $i, j$  with the coordinates  $(\phi_i, \lambda_i)$  and  $(\phi_j, \lambda_j)$ , respectively.

In the double P.M. approach, the second (deeper) layer of P.M. is located at the sphere of radius  $R'_1$  from the earth's center, where

$$R'_1 = R - d - v = R_1 - v,$$



or

$$R'_1 = R_1 + dR_1, \quad (5.3a)$$

$$dR_1 = -v. \quad (5.3b)$$

The other primed values are

$$F'_{ij} = R R'_1 \cos \psi_{ij}, \quad (5.4a)$$

$$\ell'_{ij} = (R^2 + R'^2_1 - 2F'_{ij})^{1/2}. \quad (5.4b)$$

The  $j$ -th scaled P.M. corresponding to  $R'_1$  has the magnitude  $(kM)'_j$  such that

$$(kM')_j = -(kM)_j. \quad (5.5)$$

The value of the geoid undulation due to the deeper point masses is

$$N'_i = (1/G) \sum_j (1/\ell'_{ij})(kM)'_j.$$

Upon taking (5.5) into account, the value corresponding to double point masses (at depths  $R_1$  and  $R'_1$ ) is

$$\tilde{N}_i = N_i + N'_i,$$

i.e.,

$$\tilde{N}_i = (1/G) \sum_j (1/\ell_{ij} - 1/\ell'_{ij})(kM)_j. \quad (5.6)$$

The formation of observation equations, etc., could proceed in line with Chapter 4 of [B] in conjunction with any observational mode. In particular, a row in the matrix  $A$  as described in Section 4.1 of [B] could be formed by omitting  $(kM)_j$  and utilizing the indices  $j$  to determine the ordering of the elements in this matrix.

The gravity anomaly at  $i$  due to the single point masses is

$$\Delta g_i = (1/R) \sum_j (1/\ell_{ij}) [(R^2 - F_{ij})/\ell_{ij}^2 - 2] (kM)_j, \quad (5.7)$$

as can be gathered from (4.19) of [B]. In analogy to the above, the gravity anomaly in the double P.M. approach is

$$\Delta \tilde{g}_i = (1/R) \sum_j \{ (1/\ell_{ij}) [(R^2 - F_{ij})/\ell_{ij}^2 - 2] - (1/\ell'_{ij}) [(R^2 - F'_{ij})/\ell'^2_{ij} - 2] \} (kM)_j. \quad (5.8)$$

The deflections of the vertical,  $\xi_i$  and  $\eta_i$ , in the single P.M. approach read (see 4.24 and 4.25 in [B]):

$$\xi_i = -(R_1/G) \sum_j (1/\ell_{ij}^3) [\cos\phi_i \sin\phi_j - \sin\phi_i \cos\phi_j \cos(\lambda_i - \lambda_j)] (kM)_j, \quad (5.9a)$$

$$\eta_i = (R_1/G) \sum_j (1/\ell_{ij}^3) \cos\phi_j \sin(\lambda_i - \lambda_j) (kM)_j. \quad (5.9b)$$

The corresponding expressions in the double P.M. approach are

$$\tilde{\xi}_i = -(1/G) \sum_j (R_1/\ell_{ij}^3 - R'_1/\ell'^3_{ij}) [\cos\phi_i \sin\phi_j - \sin\phi_i \cos\phi_j \cos(\lambda_i - \lambda_j)] (kM)_j, \quad (5.10a)$$

$$\tilde{\eta}_i = (1/G) \sum_j (R_1/\ell_{ij}^3 - R'_1/\ell'^3_{ij}) \cos\phi_j \sin(\lambda_i - \lambda_j) (kM)_j. \quad (5.10b)$$

The horizontal gradients of gravity disturbance,  $T_{zx_i}$  and  $T_{zy_i}$ , in the single P.M. approach read (see 4.28 and 4.29 in [B]):

$$T_{zx_i} = -3R_1 \sum_j (1/\ell_{ij}^5) (R - R_1 \cos\psi_{ij}) [\cos\phi_i \sin\phi_j - \sin\phi_i \cos\phi_j \cos(\lambda_i - \lambda_j)] (kM)_j, \quad (5.11a)$$

$$T_{zy_i} = 3R_1 \sum_j (1/\ell_{ij}^5)(R - R_1 \cos\psi_{ij})\cos\phi_j \sin(\lambda_i - \lambda_j)(kM)_j . \quad (5.11b)$$

In the double P.M. approach the corresponding expressions are

$$\begin{aligned} \tilde{T}_{zx_i} = -3 \sum_j [ & (R_1/\ell_{ij}^5)(R - R_1 \cos\psi_{ij}) - (R'_1/\ell'_{ij}{}^5)(R - R'_1 \cos\psi_{ij})] \\ & \cdot [\cos\phi_i \sin\phi_j - \sin\phi_i \cos\phi_j \cos(\lambda_i - \lambda_j)](kM)_j , \end{aligned} \quad (5.12a)$$

$$\begin{aligned} \tilde{T}_{zy_i} = 3 \sum_j [ & (R_1/\ell_{ij}^5)(R - R_1 \cos\psi_{ij}) - (R'_1/\ell'_{ij}{}^5)(R - R'_1 \cos\psi_{ij})] \\ & \cdot \cos\phi_j \sin(\lambda_i - \lambda_j)(kM)_j . \end{aligned} \quad (5.12b)$$

The vertical gradient of gravity disturbance at  $i$  in the single P.M. approach reads (see 4.31 in [B]):

$$T_{zz_i} = \sum_j (1/\ell_{ij}^3) [3(R - R_1 \cos\psi_{ij})^2/\ell_{ij}^2 - 1](kM)_j . \quad (5.13)$$

In the double P.M. approach the corresponding expression is

$$\begin{aligned} \tilde{T}_{zz_i} = \sum_j \{ & (1/\ell_{ij}^3) [3(R - R_1 \cos\psi_{ij})^2/\ell_{ij}^2 - 1] - (1/\ell'_{ij}{}^3) [3(R - R'_1 \cos\psi_{ij})^2/\ell'_{ij}{}^2 \\ & - 1] \} (kM)_j . \end{aligned} \quad (5.14)$$

Next, a decision regarding a cut-off distance when adjusting a double P.M. model will be made, again along the lines of [B], Chapter 4. In this analysis, one twin point mass will be considered,  $(kM)_j$  and  $(kM)'_j$ , in conjunction with the observation point  $i$  on the earth's surface (here a sphere of radius  $R = 6,371$  km). The depth ( $d$ ) of the shallower P.M. is taken, in agreement with the previous chapter, as a 0.8-multiple of the

horizontal separation ( $s$ ) between the twin point masses. Thus, if the horizontal separation in degrees is  $s^0 = 4^0$ , then

$$s \approx 445 \text{ km} ,$$

$$d = 0.8s \approx 350.0 \text{ km} ,$$

$$R_1 = 6,021 \text{ km} .$$

The vertical separation between the twin P.M. is chosen as

$$v = 50 \text{ km} ,$$

from which it follows that

$$R'_1 = 5,971 \text{ km} .$$

The magnitude of  $\langle \text{km} \rangle_j$  is chosen to be a  $10^{-6}$ -part of the earth's km ( $\text{km} \approx 3.986 \times 10^{14} \text{ m}^3/\text{sec}^2$ ). Next, the position of the observation point  $i$  is varied and the corresponding value  $\tilde{N}_i$  computed. This variation can proceed by selected multiples of  $s$ , which make it possible to see at how many  $s$ -intervals away from the observation point the P.M. parameters will still significantly affect the modeled value (and vice versa) and should thereby be included in the observation equation or in the prediction formulas. In theory one would include all of the P.M. parameters in every observation equation, but this would often result in prohibitive computer run-time requirements.

If one single P.M. were considered (instead of a twin P.M.), the formulas giving  $N_i$ ,  $\Delta g_i$ , etc., would be written as they stand (see 5.1, 5.7, etc.), except that the symbol  $\sum_j$  would be left out. In general, any

such observable quantity at  $i$  can be symbolized by " $O_i$ " and the coefficient of  $(KM)_j$  can be denoted " $C_{ij}$ ", so that

$$O_i = C_{ij}(KM)_j ,$$

where  $C_{ij}$  is readily gathered from the pertinent formulas. Considering the twin point masses, one has

$$\tilde{O}_i = (C_{ij} - C'_{ij})(KM)_j .$$

If this model is linearized -- and thus the analysis is concerned with relatively small separations between the twin P.M. along the vertical -- it follows from (5.3b) that

$$\tilde{O}_i = -(\partial C_{ij} / \partial R_1)(KM)_j dR_1 \equiv (\partial C_{ij} / \partial R_1)(KM)_j v .$$

This expression will now be examined in the context of all of the observational modes listed at the outset.

For the geoid undulation  $\tilde{N}_i$ , the model  $C_{ij}$  reads

$$C_{ij} = (1/G)(1/\ell_{ij}) .$$

The straightforward differentiation yields

$$\partial C_{ij} / \partial R_1 = (1/G)(1/\ell_{ij}) a_{ij} , \quad (5.15)$$

where

$$a_{ij} = -(R_1 - R \cos \psi_{ij}) / \ell_{ij}^2 , \quad (5.16)$$

and where  $\psi_{ij}$ , the angular separation between the points  $i$  and  $j$ , is taken in terms of  $n$ -multiples of  $s$  (in angular measure). The approximate results for  $\tilde{N}_i$  are presented as follows:

$n = 0 \quad \dots \quad 16.6 \text{ m (100\%)}$	$n = 1.5 \quad \dots \quad 1.6 \text{ m (10\%)}$
$n = 0.5 \quad \dots \quad 10.1 \text{ m (61\%)}$	$n = 2 \quad \dots \quad 0.7 \text{ m (4\%)}$
$n = 1 \quad \dots \quad 4.0 \text{ m (24\%)}$	$n = 2.5 \quad \dots \quad 0.4 \text{ m (2\%)}$

At the distance  $1s$  (corresponding here to  $4^\circ$ ) the effect of the twin P.M. has diminished to about 24% of the maximum effect exercised directly underneath the observation point (at  $n=0$ ). The corresponding distance could be adopted as a cut-off distance with regard to both observations and predictions. Clearly, the influence of the twin P.M. on the value of  $\tilde{N}_i$  decreases much more rapidly than is the case with the single P.M. approach summarized in Section 3.1, where, for example,  $n=2$  still corresponds to an effect as large as 37.6%.

The model for the gravity anomaly  $\Delta\tilde{g}_i$  reads

$$\begin{aligned} C_{ij} &= (1/R)(1/\ell_{ij})b_{ij} , \\ b_{ij} &= (R^2 - F_{ij})/\ell_{ij}^2 - 2 , \end{aligned} \quad (5.17)$$

which yields

$$\partial C_{ij} / \partial R_1 = (1/R_1)(1/\ell_{ij}) (a_{ij}b_{ij} + a_{ij}c_{ij} - r_{ij}) , \quad (5.18)$$

$$c_{ij} = 2(R^2 - F_{ij})/\ell_{ij}^2 \equiv 2(b_{ij} + 2) , \quad (5.19)$$

$$r_{ij} = R \cos\psi_{ij} / \ell_{ij}^2 . \quad (5.20)$$

The approximate results for  $\Delta\tilde{g}_i$  are

$$\begin{array}{ll} n = 0 & \dots 88.0 \text{ mgal (100\%)} \\ n = 0.5 & \dots 30.4 \text{ mgal (34\%)} \end{array} \quad \begin{array}{ll} n = 1 & \dots 0.9 \text{ mgal (1\%)} \\ n = 1.5 & \dots -1.9 \text{ mgal (-2\%)} \end{array}$$

At the distance of merely 0.5s (here  $2^\circ$ ) the percentage is already down to 34% and, even more importantly, it decreases so rapidly that at  $n=1$  it is 1%. A cut-off decision made in favor of  $n=1$  would be more than sufficient. By comparison, in the single P.M. approach  $n=1$  corresponds to 21.4%.

Similar to [B], the analysis of the deflections of the vertical leads to the same results whether  $\tilde{\xi}_i$  or  $\tilde{\eta}_i$  is considered. The case with  $\tilde{\eta}_i$  yields

$$\begin{aligned} C_{ij} &= (R_1/G)(1/\ell_{ij}^3)s_{ij} , \\ s_{ij} &= \cos\phi_j \sin(\lambda_i - \lambda_j) , \end{aligned} \quad (5.21)$$

where the point  $j$  is considered at the equator, thus  $\cos\phi_j = 1$ . Subsequently, one has

$$\partial C_{ij} / \partial R_1 = (R_1/G)(1/\ell_{ij}^3)s_{ij}(1/R_1 + 3a_{ij}) . \quad (5.22)$$

The approximate results pertaining to  $\tilde{\eta}_i$  (or  $\tilde{\xi}_i$ ) are

$$\begin{array}{ll} n = 0 & \dots 0.0'' \text{ (0\%)} \\ n = 0.5 & \dots 8.0'' \text{ (100\%)} \\ n = 1 & \dots 3.5'' \text{ (44\%)} \end{array} \quad \begin{array}{ll} n = 1.5 & \dots 1.3'' \text{ (16\%)} \\ n = 2 & \dots 0.5'' \text{ (6\%)} \\ n = 2.5 & \dots 0.2'' \text{ (3\%)} \end{array}$$

A cut-off distance at 1.5s (here  $6^\circ$ ) would be more than sufficient,

corresponding to about 16% of the maximum effect for  $n \approx 0.5$ . By comparison, the single P.M. approach shows about the same effect (more precisely 17.1%) for  $n = 3s$ .

The analysis of the horizontal gradients of gravity disturbance produces the same results for either  $\tilde{T}_{zx}$  or  $\tilde{T}_{zy}$  gradient. The case with  $\tilde{T}_{zy_i}$  yields

$$\begin{aligned} C_{ij} &= 3R_1(1/\ell_{ij}^5)u_{ij}s_{ij} , \\ u_{ij} &= R - R_1 \cos\psi_{ij} , \end{aligned} \quad (5.23)$$

where  $j$  is again taken at the equator; thus

$$\partial C_{ij}/\partial R_1 = 3R_1(1/\ell_{ij}^5)u_{ij}s_{ij}(1/R_1 + 5a_{ij} - \cos\psi_{ij}/u_{ij}) . \quad (5.24)$$

The approximate results in  $E$  (Eötvös, 0.1 mgal/km or  $10^{-9} \text{ sec}^{-2}$ ) pertaining to  $\tilde{T}_{zy_i}$  (or  $\tilde{T}_{zx_i}$ ) are

$n = 0$	... 0.00 $E$ ( 0%)	$n = 1$	... 0.49 $E$ (14%)
$n = 0.25$	... 3.45 $E$ (100%)	$n = 1.5$	... 0.03 $E$ ( 1%)
$n = 0.5$	... 2.86 $E$ ( 83%)	$n = 2$	... -0.02 $E$ (-0.5%)

A cut-off distance at  $1s$  (here  $4^\circ$ ) would be more than sufficient, corresponding to about 14% of the maximum effect at  $n \approx 0.25$ . By comparison, the single P.M. approach shows about the same effect (more precisely 17.2%) for  $n = 1.5$ .



The model for the vertical gradient of gravity disturbance  $\tilde{T}_{zz_i}$  yields

$$C_{ij} = (1/\ell_{ij}^3)(3u_{ij}^2/\ell_{ij}^2 - 1) ,$$

$$\partial C_{ij}/\partial R_1 = 3(1/\ell_{ij}^3)[(5u_{ij}^2/\ell_{ij}^2 - 1)a_{ij} - 2u_{ij}\cos\psi_{ij}/\ell_{ij}^2] . \quad (5.25)$$

The approximate results for  $\tilde{T}_{zz_i}$  are

$n = 0$	... 7.96 E (100%)	$n = 1$	... -0.35 E (-4%)
$n = 0.5$	... 1.16 E (15%)	$n = 1.5$	... -0.18 E (-2%)

A cut-off distance at 0.5s (here  $2^\circ$ ) appears more than sufficient, and it corresponds to about 15% of the maximum effect at  $n=0$ . By comparison, the single P.M. approach shows a 37.5% effect for the same distance.

## 5.2 Development of Deflection Rates in Terms of Twin Point Masses

The development in this section is based on the results from Section 4.3, where the model for deflection rates has been formulated in terms of single point masses. The notations of the previous section are adopted without changes, with primes indicating the quantities connected with the deeper layer of the point masses, "~" designating the quantities resulting from the effect of both layers of point masses,  $v$  denoting the vertical separation of the twin point masses, etc. Again, the twin point masses have the same mass magnitude but the opposite sign. Thus, from (4.18) and (4.19) we write the basic model for the deflection rates as follows:

$$\begin{aligned}\tilde{\xi}_i = & (R_1/GR) \sum_j \{ [(1/\ell_{ij}^3)(p_{ij} t_{ij} - \text{tg}\phi_i) - (1/\ell'_{ij}{}^3)(p'_{ij} t_{ij} - \text{tg}\phi_i)] \\ & \cdot (q_{ij}/\cos\phi_i)\sin\alpha - [(1/\ell_{ij}^3)(p_{ij} t_{ij}^2 - \cos\psi_{ij}) \\ & - (1/\ell'_{ij}{}^3)(p'_{ij} t_{ij}^2 - \cos\psi_{ij})]\cos\alpha\}(kM)_j, \quad (5.26)\end{aligned}$$

$$\begin{aligned}\tilde{\eta}_i = & (R_1/GR \cos\phi_i) \sum_j \{ [(1/\ell_{ij}^3)(p_{ij} q_{ij}^2 - \cos\phi_i \cos\phi_j \cos\Delta\lambda_{ij}) \\ & - (1/\ell'_{ij}{}^3)(p'_{ij} q_{ij}^2 - \cos\phi_i \cos\phi_j \cos\Delta\lambda_{ij})](1/\cos\phi_i)\sin\alpha \\ & - (p_{ij}/\ell_{ij}^3 - p'_{ij}/\ell'_{ij}{}^3)q_{ij} t_{ij} \cos\alpha\}(kM)_j, \quad (5.27)\end{aligned}$$

where the trigonometric functions associated with the deeper point mass are unchanged when passing to the primed quantities, including  $\cos\psi_{ij}$ ,  $t_{ij}$  and  $q_{ij}$ , but where

$$p'_{ij} = 3RR'_1/\ell'^2_{ij}.$$

As in the approach with the single point masses in Section 4.3, we consider only the effect of one P.M. magnitude located at the point  $j$  (where  $\phi_j=0$ ) on the model value at the (observation) point  $i$ . Adopting also the previous notations and approximations, we can derive -- or transcribe from (4.20) and (4.20') -- the following relations:

$$\begin{aligned} \tilde{\xi}_i = & -(R_1/GR)\{(p_{ij}/\ell^3_{ij} - p'_{ij}/\ell'^3_{ij})\Delta\phi_{ij}\Delta\lambda_{ij}\sin\alpha + [(p_{ij}/\ell^3_{ij} - p'_{ij}/\ell'^3_{ij})\Delta\phi^2_{ij} \\ & - (1/\ell^3_{ij} - 1/\ell'^3_{ij})]\cos\alpha\}(\kappa M)_j, \end{aligned} \quad (5.28)$$

$$\begin{aligned} \tilde{\eta}_i = & -(R_1/GR)\{[(p_{ij}/\ell^3_{ij} - p'_{ij}/\ell'^3_{ij})\Delta\lambda^2_{ij} - (1/\ell^3_{ij} - 1/\ell'^3_{ij})]\sin\alpha \\ & + (p_{ij}/\ell^3_{ij} - p'_{ij}/\ell'^3_{ij})\Delta\phi_{ij}\Delta\lambda_{ij}\cos\alpha\}(\kappa M)_j; \end{aligned} \quad (5.28')$$

the comment made in conjunction with (4.20) and (4.20') can be adopted, word for word, also in the present situation as depicted in the above two equations. Accordingly, only (5.28) will be examined with respect to  $\alpha$  and  $\beta$ .

With regard to the vertical separation, we adopt

$$v = 0.112s,$$

which corresponds to  $v=50$  km for  $s=445$  km (this, in turn, corresponds to  $4^\circ$ ). Thus, recalling that in angular measure  $s$  has been denoted as  $\Delta\omega$ , we have

$$d' = d + v = 0.912s = 0.912 R \Delta\omega, \quad d'^2 = 0.83 R^2 \Delta\omega^2 .$$

If the value 0.64 in the formulas (4.22) is replaced by 0.83, it can readily be shown that

$$\left. \begin{aligned} 1/\ell_{ij}^3 - 1/\ell'_{ij}{}^3 &\approx (1/R^3 \Delta\omega^3) [0.285/(n^2 + 0.64)^{5/2}] , \\ p_{ij}/\ell_{ij}^3 - p'_{ij}/\ell'_{ij}{}^3 &\approx (1/R^3 \Delta\omega^5) [1.425/(n^2 + 0.64)^{7/2}] , \end{aligned} \right\} \quad (5.29)$$

provided  $0.83 - 0.64 = 0.19$  can be considered small compared to  $n^2 + 0.64$ , which is quite acceptable for the values we are most interested in (between  $n=1$  and  $n=2$ ). The relations in (5.29) are derived from

$$d(1/x)^{k/2} = -(k/2)(1/x)^{k/2+1}dx ,$$

with  $x=n^2 + 0.64$ ,  $dx=0.19$  and  $k=3$  or  $5$ .

If (5.28) is developed with the aid of (5.29), as well as with the notations introduced in (4.21), it follows that

$$\begin{aligned} \tilde{\zeta}_i &= -C[1/(n^2 + 0.64)^{7/2}] [1.425n^2 \sin\beta \cos\beta \sin\alpha \\ &\quad + (1.425n^2 \cos^2\beta - 0.285n^2 - 0.182) \cos\alpha] , \end{aligned} \quad (5.30)$$

where C is the same as in (4.23'). Since in view of (4.24), (4.24') we again have  $a=b$ , an extreme for the function in the second brackets above does not exist, and we proceed to examine  $\alpha=0$ ,  $45^\circ$  and  $90^\circ$ , searching now for extremes with respect to  $\beta$ . The strategy used for the single point masses will be pursued here as well.

Azimuth  $\alpha=0$ . In exact analogy to Section 4.3, a maximum occurs at  $\beta=0$  which now coincides with an absolute maximum already for  $n>0.65$  (previously this held true for  $n>1.13$ ). Parallel to (4.25) and (4.25') we have

$$\alpha=0, \quad \beta=0; \quad \tilde{\xi}_i = -C[(1.140n^2 - 0.182)/(n^2 + 0.64)^{7/2}]; \quad (5.31)$$

$n = 0$	.....	100%	$n = 1$	.....	-19.5%	}	(5.31')
$n = 0.5$	.....	-17.8%	$n = 1.5$	.....	-6.7%		
$n = 0.69$	.....	-28.3%	$n = 2$	.....	-2.3%		

Note: In addition to the primary maximum at  $n=0$ , a secondary maximum exists at  $n=0.69$ . Beyond  $n=1$  the values in (5.31') are seen to decrease much more rapidly than their counterparts in (4.25').

Azimuth  $\alpha=45^\circ$ . A maximum occurs at  $\beta=22.5^\circ$  as in Section 4.3, but it now corresponds to an absolute maximum already for  $n>0.56$  (as opposed to  $n>0.89$  found previously). In analogy to (4.26) and (4.26') we have

$$\alpha=45^\circ, \quad \beta=22.5^\circ; \quad \tilde{\xi}_i = -C[(1.435n^2 - 0.182)/(n^2 + 0.64)^{7/2}]; \quad (5.32)$$

$n = 0$	.....	100%	$n = 1$	.....	-25.6%	} (5.32')
$n = 0.5$	.....	-30.6%	$n = 1.5$	.....	-8.6%	
$n = 0.66$	.....	-39.6%	$n = 2$	.....	-3.0%	

Note: In addition to the primary maximum at  $n=0$ , a secondary maximum exists at  $n=0.66$ . Beyond  $n=1$ , the values in (5.32') decrease much more rapidly than their counterparts in (4.26'), similar to the previous case.

Azimuth  $\alpha=90^\circ$ . Here again, the (absolute) maximum at  $\beta=45^\circ$  corresponds to its single P.M. counterpart. Similar to (4.27) and (4.27'), the results are

$$\alpha=90^\circ, \quad \beta=45^\circ; \quad \tilde{\xi}_1 = -C[0.712n^2/(n^2 + 0.64)^{7/2}]; \quad (5.33)$$

$n = 0$	.....	0	$n = 1$	.....	-47.1%	} (5.33')
$n = 0.5$	.....	-100%	$n = 1.5$	.....	-14.6%	
			$n = 2$	.....	-4.9%	

Note: The formula (5.33) reveals only the (primary) maximum at  $n=0.5$  (more precisely at  $n=0.51$ ).

The case  $\alpha=90^\circ$  is again much "worse" than  $\alpha=45^\circ$  which, in turn, is only slightly "worse" than  $\alpha=0$ . This is, accordingly, the "worst situation" as discussed previously in Section 4.3 dealing with the single point masses. But even for  $\alpha=90^\circ$  the cut-off distance of 1.5s is more than sufficient (it is associated with 14.6% while in the single P.M. approach we had 43.7%). We can again summarize this development by stating that the "worst situation" occurs for  $\tilde{\xi}_1$  at  $\alpha=90^\circ$  or for  $\tilde{\eta}_1$  at  $\alpha=0$ , with  $\beta=45^\circ$  in both cases.

## 6. CONCLUSIONS

The simultaneous global adjustment of satellite altimeter data in terms of spherical-harmonic (S.H.) potential coefficients, tidal parameters and state vector (s.v.) components results in a smooth approximation to the oceanic geoid, called the trend surface, and in the residuals containing the suppressed geoidal detail. In addition to the trend surface, the adjusted S.H. coefficients can express other features of the smoothed-out global gravity field. For example, predicted values of gravity anomalies, deflections of the vertical and other functions of the disturbing potential can be computed in a desired grid from which contour maps can be constructed, etc.

The satellite altimeter adjustments recently performed at AFGL are based on the short-arc algorithm, where the arcs' lengths have been limited to seven minutes or less and the data consist of SEASAT altimeter observations. Each satellite arc is described by six s.v. parameters considered independent from arc to arc. The tidal parameters consist of a global amplitude factor and a global phase angle correction for each diurnal and semidiurnal constituent included in the adjustment. Each long-period constituent has been attributed only the first parameter. The simultaneous adjustment with an unlimited number of arcs is feasible only by virtue of eliminating the s.v. parameters from the normal equations as soon as the last observation on a given arc has been processed, and of re-using the same core space for the next arc. The short-arc algorithm as well as the weighting of altimeter observations and all three groups of parameters have been described in the previous AFGL reports.

The (weighted) tidal parameters are shown in Chapter 2 to be essentially uncontaminated by the geoidal errors or by the systematic orbital errors. The insensitivity of these parameters to the geoidal errors stems from the time-dependent properties of the former contrasted to the time invariability of the latter. And the insensitivity of these parameters to the systematic orbital errors stems from the global properties of the former contrasted to the local character of the latter (the systematic errors change from one area to another). Such advantages do not exist in a model where the adjustment is made in terms of S.H. tidal coefficients. Although the a priori values of such coefficients are used in the present model to describe the approximate behavior of the pertinent diurnal or semidiurnal constituent, only two of their very special linear combinations represented by the above two tidal parameters are subject to adjustment. Clearly, non-adjustable coefficients cannot be affected by orbital or other systematic errors.

Chapter 2 also illustrates the improvements in the trend surface, geoidal residuals and "observed" geoid undulations due to the inclusion of the tidal adjustment in the overall adjustment of satellite altimetry. The geoidal residuals can be used as observations in a subsequent, or second-phase, adjustment of a short-wavelength oceanic geoid in terms of point-mass (P.M.) magnitudes as parameters. And the "observed" geoid undulations, obtained by superimposing the geoidal residuals on the trend surface, can serve in describing the geoidal detail in yet another fashion. As one example, they can be used to produce a high-degree and order set of S.H. potential coefficients via integral formulas (not via an adjustment), which can then



serve in predicting the desired geophysical quantities. Further properties and uses of the geoidal residuals and "observed" geoid undulations are listed in the latter part of Chapter 2.

Chapter 3 is concerned with a reformulation of the second-phase adjustment in terms of P.M. parameters, leading to a banded system of normal equations. Such a system can be arrived at and resolved by addressing three separate tasks. The first task is to eliminate a number of point masses from a given observation equation. However, these point masses should be located sufficiently far from the pertinent observation point so that the rigor of the solution not be unduly compromised. Due to the bandwidth considerations, the cut-off distance should be as small as practicable. This, in turn, implies that the depth/side ratio characterizing the P.M. distribution should be reasonably small. As a result, the 1.6/1 ratio used recently has been lowered to a 0.8/1 ratio. The second task is to arrange the P.M. parameters in such a way that a banded structure may indeed materialize. The first task alone would merely lead to a great number of zeros in the normal equations, not necessarily to their banded structure. And the third task is to solve the resulting system with a maximum efficiency through an adaptation of the well-known Choleski algorithm.

The combined solution to the three tasks above gives rise to a "modified Choleski algorithm". Whereas previously only small areas could be resolved in a P.M. approach, the oceanic geoid over entire ocean basins can now be adjusted in a few overlapping strips of point masses. Indeed, the modified Choleski algorithm reduces both the run-time and the core-space requirements several fold. For example, 1,300 point masses can be deployed

with this algorithm as compared to about 200 point masses which would have been admissible otherwise.

In Chapter 4 a model for the deflection rates along a given route is developed in tensor notations, and is subsequently specialized for the S.H. and P.M. parameters. It is pointed out that the rate of change in the north deflection of the vertical ( $\xi$ ) when proceeding eastward is not the same as the rate of change in the east deflection of the vertical ( $\eta$ ) when proceeding northward. However, the difference between these two rates is expressed in a simple relationship which can serve as a useful verification. The formulas developed in terms of the S.H. potential coefficients are verified in Chapter 4 and the formulas developed in terms of the P.M. parameters are verified in the Appendix. Chapter 4 closes with an analysis of a cut-off distance under varying circumstances. It is concluded that even in the worst case situation the approximations associated with a recommended cut-off distance are somewhat less serious than the approximations associated with the same distance in the case of geoid undulations.

Chapter 5 transforms the observational modes developed and described in the previous AFGL reports from the context of single point masses to the context of twin point masses (the former implies a single P.M. layer while the latter implies a double P.M. layer). These modes are: geoid undulations, gravity anomalies, deflections of the vertical (north and east), horizontal gradients of gravity disturbance (north and east), and vertical gradients of gravity disturbance. In the latter part of Chapter 5 the same transformation takes place also for the newly developed deflection rates. The deflection rate formulas in terms of twin P.M. parameters can be verified in close

analogy to their single P.M. counterparts. Since the same verification takes place for the upper and the lower point mass, and since the contributions of these two point masses are added algebraically, the pertinent formulas in the twin P.M. model are automatically verified. An analysis of all the observational modes considered confirms the plausible property that if a single point mass is made into a twin point mass, the effect exercised on a modeled value decreases much more rapidly with distance.

# APPENDIX

## VERIFICATION OF THE POINT-MASS MODEL FOR THE DEFLECTION RATES

The verification formula (4.8) for the deflection rates, applied at the observation point  $i$ , reads

$$\dot{\xi}_{E_i} - \dot{\eta}_{N_i} = (1/GR^2 \cos \phi_i) \operatorname{tg} \phi_i \partial T_i / \partial \lambda_i ,$$

where  $\partial T_i / \partial \lambda_i$  is given in [Blaha, 1980], equation (4.7b), as

$$\partial T_i / \partial \lambda_i = -RR_1 \cos \phi_i \sum_j (1/\ell_{ij}^3) \cos \phi_j \sin \Delta \lambda_{ij} (km)_j ,$$

with  $\Delta \lambda_{ij}$  denoting  $\lambda_i - \lambda_j$  as before. We then have

$$\dot{\xi}_{E_i} - \dot{\eta}_{N_i} = -(R_1/GR) \operatorname{tg} \phi_i \sum_j (1/\ell_{ij}^3) \cos \phi_j \sin \Delta \lambda_{ij} (km)_j . \quad (A.1)$$

On the other hand, the formula (4.18) with  $\alpha=90^\circ$  and the formula (4.19) with  $\alpha=0$  yield respectively:

$$\begin{aligned} \dot{\xi}_{E_i} &= (R_1/GR \cos \phi_i) \sum_j (1/\ell_{ij}^3) (p_{ij} t_{ij} - \operatorname{tg} \phi_i) q_{ij} (km)_j , \\ \dot{\eta}_{N_i} &= (R_1/GR \cos \phi_i) \sum_j (1/\ell_{ij}^3) p_{ij} q_{ij} t_{ij} (km)_j , \end{aligned}$$

and thus

$$\dot{\xi}_{E_i} - \dot{\eta}_{N_i} = -(R_1/GR \cos \phi_i) \sum_j (1/\ell_{ij}^3) \operatorname{tg} \phi_i q_{ij} (km)_j . \quad (A.2)$$

But due to the notation introduced following (4.19), namely

$$q_{ij} = \cos\phi_i \cos\phi_j \sin\Delta\lambda_{ij} ,$$

equation (A.2) becomes (A.1) and the verification is terminated.

## ACKNOWLEDGEMENT

Dr. Urho A. Rauhala of Geodetic Services, Inc., Melbourne, Florida, is acknowledged for discussions on the topic of banded systems of normal equations as used in the field of photogrammetry; he in turn benefitted from the experience and work of Professor Ebner of Technical University in Munich.

## REFERENCES

- Blaha, G., Improved Determinations of the Earth's Gravity Field. AFGL Technical Report No. 79-0058, Air Force Geophysics Laboratory, Hanscom AFB, Massachusetts, 1979, ADA070186.
- Blaha, G., Extended Applicability of the Spherical-Harmonic and Point-Mass Modeling of the Gravity Field. AFGL Technical Report No. 80-0180, Air Force Geophysics Laboratory, Hanscom AFB, Massachusetts, 1980, ADA089072.
- Blaha, G., SEASAT Altimetry Adjustment Model Including Tidal and Other Sea Surface Effects. AFGL Technical Report No. 81-0152, Air Force Geophysics Laboratory, Hanscom AFB, Massachusetts, 1981, ADA104188.
- Blaha, G., Modeling and Adjusting Global Ocean Tides Using SEASAT Altimeter Data. AFGL Technical Report No. 82-0114, Air Force Geophysics Laboratory, Hanscom AFB, Massachusetts, 1982, ADA115841.
- Estes, R.H., "A Simulation of Global Ocean Tide Recovery Using Altimeter Data with Systematic Orbit Error". Paper published in Marine Geodesy, Volume 3, Nos. 1-4, Crane Russak, New York, 1980.
- Hotine, M., Mathematical Geodesy. Monogr. Ser., Vol. 2, Environ. Sci. Serv. Admin., Washington, D.C., 1969.
- Heiskanen, W.A. and H. Moritz, Physical Geodesy. W.H. Freeman and Co., San Francisco, 1967.
- Needham, P.E., The Formation and Evaluation of Detailed Geopotential Models Based on Point Masses. Department of Geodetic Science, Report No. 149, The Ohio State University, Columbus, 1970.
- Parke, M.E. and M.C. Hendershott, "M2, S2, K1 Models of the Global Ocean Tide on an Elastic Earth". Paper published in Marine Geodesy, Volume 3, Nos. 1-4, Crane Russak, New York, 1980.
- Schwiderski, E.W., "Ocean Tides, Part I: Global Ocean Tidal Equations". Paper published in Marine Geodesy, Volume 3, Nos. 1-4, Crane Russak, New York, 1980.
- TOPEX Science Working Group, Satellite Altimetric Measurements of the Ocean. NASA, Jet Propulsion Laboratory of the California Institute of Technology, Pasadena, March 1, 1981.
- Vaníček, P., Tidal Corrections to Geodetic Quantities. NOAA Technical Report NOS 83 NGS 14, U.S. Department of Commerce, NOAA, NOS, Rockville, Maryland, 1980.

END

FILMED

8-83

DTIC